DOI: 10.26599/FSHW.2025.9250828

Contents lists available at SciOpen

Food Science and Human Wellness

journal homepage: https://www.sciopen.com/journal/2097-0765

China Food Publishing Co.

Ganoderic acid C2 alleviates sepsis-associated acute kidney injury via neuraminidase 1-nuclear factor erythroid 2-related factor 2-mediated ferroptosis inhibition

Shangpeng Yang[1†], Hui Fang[1*†], Chunyun Ji[1], Zumin Hou[1], Teng Yang[1], Dongmei Lin[2], Lianfu Wang[2], Hongjian Luo[2*]

[1]*School of Pharmacy, Shandong Second Medical University, Weifang 261053, Shandong, China*

[2]*National Engineering Research Center of JUNCAO Technology, Fujian Agriculture and Forestry University, Fujian Fuzhou 350002, China*

ABSTRACT: Sepsis-associated acute kidney injury (S-AKI) remains a critical clinical challenge due to its complex pathogenesis, which involves intertwined oxidative stress, ferroptosis, and inflammatory cascades. Despite advances in understanding these mechanisms, existing therapies fail to concurrently target these core pathological drivers, limiting their clinical efficacy. Here, we demonstrate that Ganoderic acid C2 (GA-C2), a triterpenoid from *Ganoderma lucidum*, inhibits neuraminidase 1 (NEU1) activity to restore nuclear factor erythroid 2-related factor 2 (Nrf2) stability and suppress ferroptosis in S-AKI models. In lipopolysaccharide-stimulated renal tubular epithelial cells and murine sepsis, GA-C2 treatment blocked NEU1-mediated Nrf2 degradation, reducing oxidative stress (via Nrf2/ glutathione peroxidase 4 axis stabilization) and inflammation (via nuclear factor-κB inhibition) while upregulating ferroptosis suppressor protein 1. Molecular docking and cellular thermal shift assays revealed GA-C2 binds directly to NEU1's catalytic pocket (ARG335/PRO310/VAL311), disrupting its ability to drive Nrf2 ubiquitination and phosphorylation. Crucially, GA-C2 outperformed classical inhibitors by simultaneously targeting both Kelch-like ECH-associated protein 1-dependent and glycogen synthase kinase 3β-driven Nrf2 degradation pathways. These results establish GA-C2 as a NEU1 inhibitor that alleviates S-AKI by coordinately restoring redox balance, suppressing ferroptosis, and attenuating inflammation. By elucidating NEU1's dual regulatory role in Nrf2 signaling, this work advances the mechanistic understanding of S-AKI and provides a blueprint for multi-target therapeutic design. Furthermore, GA-C2's efficacy and natural origin highlight the potential of *Ganoderma*-derived compounds as foundational candidates for nutraceuticals or adjunctive therapies in sepsis management, bridging the gap between mechanistic discovery and translational applications.

Keywords: *Ganoderma lucidum*; Ganoderic acid C2; Sepsis-associated acute kidney injury; Nrf2; NEU1; Ferroptosis.

1. Introduction

Sepsis-associated acute kidney injury (S-AKI) is a severe complication of systemic infection and a major clinical challenge in critical care. Data from epidemiological studies reveal that S-AKI makes up over 50% of acute kidney injury (AKI) incidents in intensive care units [1]. The mortality rate for S-AKI is strikingly high at 70.2%, and there is a direct connection between the severity of AKI progression and patient mortality [2,3].

†These authors contributed equally to this work.
***Corresponding author**
fanghui8@sdsmu.edu.cn; luohongjian14@163.com

Received 17 May 2025
Received in revised from 3 July 2025
Accepted 25 July 2025

These statistics underscore the critical need for effective therapeutic strategies to mitigate the morbidity and mortality linked to this condition. S-AKI pathogenesis is characterized by intricate mechanisms such as oxidative stress, abnormal inflammation [4,5], and ferroptosis, an iron-dependent cell death caused by lipid peroxidation [6–8]. Despite advances in sepsis management, therapies targeting these underlying pathways are still limited, emphasizing the need for novel interventions.

Neuraminidase 1 (NEU1), a mammalian sialidase that influences inflammation and redox signaling, has been recently recognized as a crucial contributor to organ injury pathogenesis [9]. NEU1 is extensively present in kidney tissues and is crucial for processes like fibrosis [10] and inflammation [11,12]. Pharmacological inhibition of NEU1 has shown promise in treating diseases like pulmonary fibrosis [13] and cardiomyopathy [14], indicating its potential as a therapeutic target. However, the role of NEU1 in S-AKI remains unexplored, despite its involvement in fibrosis, inflammation, and the mechanisms that underlie oxidative stress and ferroptosis—critical factors in the development of S-AKI.

Ganoderma lucidum, a medicinal mushroom extensively utilized in traditional Eastern medicine, is renowned for its diverse repertoire of bioactive constituents, including polysaccharides, triterpenoids, and proteins [15]. Each of these components contributes distinct pharmacological properties [16]. For example, GSBP-2, a polysaccharide isolated from *Ganoderma sinense*, has demonstrated potent antitumor efficacy in breast cancer models by modulating the Phosphoinositide 3-kinase (PI3K) / Protein Kinase B (Akt) and epithelial-mesenchymal transition signaling pathways [17,18]. In parallel, triterpenoids—particularly Ganoderic acids (GAs), which are oxidized derivatives of lanosterol—constitute a major class of bioactive compounds in *Ganoderma lucidum* [19]. GAs have been shown to ameliorate alcohol-induced liver injury by regulating gut microbiota composition and attenuating inflammatory signaling pathways [20,21]. Notably, several GAs have also demonstrated protective effects in AKI models, particularly those induced by ischemia-reperfusion injury [22]. Among these, Ganoderic acid C2 (GA-C2) has emerged as a promising candidate due to its potent antioxidant and anti-inflammatory properties [23,24]. Nevertheless, the precise molecular mechanisms underlying GA-C2's renal protective effects—especially in the context of S-AKI—remain poorly defined. In particular, its potential interaction with NEU1 and involvement in ferroptosis signaling has not been elucidated.

In sepsis, the accumulation of iron, depletion of glutathione (GSH), and inhibition of glutathione peroxidase 4 (GPX4) collaboratively promote ferroptosis in renal tubular epithelial cells. Additionally, the inactivation of the nuclear factor erythroid 2-related factor 2 (Nrf2) pathway is pivotal in driving the progression of S-AKI [25]. In lipopolysaccharide (LPS)-induced acute lung injury, Nrf2, a critical regulator of antioxidant defense, undergoes destabilization through Kelch-like ECH-associated protein 1 (Keap-1)-mediated ubiquitination and glycogen synthase kinase 3β (GSK3β)-dependent phosphorylation, ultimately resulting in its degradation [26]. Recent studies indicate that ferroptosis is a key mechanism in the progression of AKI [27]. Two downstream effectors of Nrf2, ferroptosis suppressor protein 1 (FSP1) and GPX4, are essential in protecting against lipid peroxidation [28]. However, Nrf2 suppression during sepsis

disrupts this protective axis, creating conditions that favor ferroptosis [7]. Interestingly, NEU1 knockdown has been shown to enhance Nrf2 target gene expression, suggesting that NEU1 represses Nrf2 signaling [29]. This suggests that targeting NEU1 may restore redox balance. Despite this rationale, no studies have explored natural compounds capable of simultaneously modulating both NEU1 and the Nrf2/ferroptosis axis in the context of S-AKI.

This study bridges food chemistry and translational medicine by exploring the mechanistic link through which GA-C2, a bioactive triterpenoid from *Ganoderma lucidum*, alleviates renal injury in S-AKI. We propose that GA-C2 exerts its renoprotective effects through a multi-target mechanism: direct inhibition of NEU1 disrupts downstream inflammatory cascades (e.g., nuclear factor-κB (NF-κB) signaling), stabilizes Nrf2 to restore redox homeostasis, and suppresses ferroptosis by upregulating GPX4 and FSP1. This hypothesis positions GA-C2 as a novel therapeutic candidate capable of simultaneously targeting the key pathological pathways of S-AKI. Using LPS-induced *in vitro* and *in vivo* sepsis models, we show that GA-C2 binds to the catalytic pocket of NEU1 (ARG335/PRO310/VAL311), disrupts its enzymatic activity, and reactivates Nrf2 through both Keap-1 and GSK3β-dependent pathways. Our findings suggest that GA-C2 acts as a dual-target therapeutic agent and holds potential as a promising functional food ingredient for the management of sepsis.

2. Materials and methods

2.1. GAs preparation

Take 1 kg of sliced *Ganoderma lucidum*, add 10 L of anhydrous ethanol (China National Pharmaceutical Group Corporation), place it in a multifunctional reactor (SENCOO Technology Co., Ltd.), stir at 15 r/min, reflux extract at 60°C for 2 hours, take out the ethanol extract, evaporate to a small amount using a rotary evaporator (R100 2B, Shanghai ShenSheng Technology Co., Ltd.), centrifuge at 1000 r/min for 10 minutes, filter the clear liquid through a 0.22 μm filter, transfer to an evaporating dish, evaporate to a paste-like state using a water bath (Jinghong Company), grind into powder after freeze-drying to obtain crude GAs extract Ganoderic acid n (GA-n).

Take 30 g of crude GAs extract GA-n, add 100 mL of anhydrous ethanol, dissolve with ultrasound. The sample undergoes filtration using a 0.22 μm disposable filter head, after which the filtrate is processed through Flash medium-pressure preparation utilizing the GRACE Reveleris Prep holistic fast purification chromatograph (Grace, USA). The first component mainly contains GA-C2 and a small amount of Ganoderic acid B (GA-B), the second component mainly contains GA-B and Ganoderic acid A (GA-A), and the third component contains various difficult-to-separate GAs, which are collected for other research purposes.

The combined first and second components are concentrated to dryness, supplemented with an appropriate amount of anhydrous ethanol, filtered through a 0.22 μm filter head, and subjected to high-pressure preparation using the GRACE Reveleris Prep holistic fast purification chromatograph (Grace, USA). The three components are separately collected, concentrated, evaporated to dryness, and recrystallized to obtain GA-C2, GA-B, GA-A. The tracking detection and purity identification results using the Waters 2535

high-performance liquid chromatograph with a 2489 ultraviolet detector (Waters, USA), with all three GAs having a purity of over 98%. The structures of the three compounds, as identified by the third-party Institute of Materia Medica, Chinese Academy of Medical Sciences & Peking Union Medical College.

2.2. Ethical statement

Male C57BL/6 mice were sourced from Pengyue Experimental Animal Breeding Co., Ltd., located in Jinan, China. The animal experiments were carried out by personnel trained at the Center for Experimental Animals, Shandong Second Medical University. All procedures were conducted in compliance with ethical guidelines and were approved under license number 2023SDL340. To minimize animal distress, all surgical interventions were performed under 2%-3% isoflurane anesthesia.

2.3. Drug preparation and administration

In the animal experiments, GAs were dissolved in a saline solution containing 5% Tween 80. The drug, or an equivalent volume of the vehicle, was administered intraperitoneally once daily over a period of three consecutive days. Subsequent to the final drug administration, an injection of LPS was administered. Ferrostatin-1 (Fer-1, IF0430, Solarbio, 10 mg/kg), ML385 (IM1020, Solarbio, 30 mg/kg), and tert-Butylhydroquinone (TBHQ, SB8960, Solarbio, 50 mg/kg) were dissolved in dimethyl sulfoxide (DMSO, D8371, Solarbio) and administered intraperitoneally at intervals of 1 hour, 2 hours, and 8 hours prior to the LPS injection (L8880, Solarbio, 10 mg/kg). The concentration of DMSO was maintained below 2.5%.

In vitro experiments involved dissolving GAs in DMSO, diluting it to the required concentration in culture medium, and applying it to rat proximal renal tubular (NRK-52E) cells. ML385 (20 μmol/L) and TBHQ (30 μmol/L) were also dissolved in DMSO and added to the cells before LPS exposure (1 μg/mL). The DMSO concentration was kept below 0.1% in all experimental groups.

2.4. Experimental grouping

C57BL/6 mice underwent a one-week acclimation period in a 12-hour light/dark cycle, with unrestricted food and water access. According to established protocols [22,30], the mice were randomly sorted into the following groups: Control (CTR), LPS, LPS + low dose of Ganoderic acid n (GA-n-L), LPS + high dose of Ganoderic acid n (GA-n-H), LPS + GA-A, LPS + GA-B, LPS + GA-C2, LPS + Fer-1, LPS + TBHQ, LPS + GA-n-H + ML385, and LPS + GA-C2 + ML385. Each group consisted of six mice (n=6).

Upon conclusion of the experimental procedure, the mice were anesthetized with 2%-3% isoflurane. Subsequently, body weight measurements were obtained, blood samples were collected from the inferior vena cava, and kidney specimens were excised and weighed. The kidneys were then sectioned into two portions: one portion was rapidly frozen in liquid nitrogen for subsequent protein analysis via western blotting, while the other portion was processed for paraffin embedding to facilitate morphological examination.

2.5. Cell culture

The NRK-52E rat proximal tubular epithelial cell line (CL-0174, Procell Life Science & Technology Co., Ltd.) was cultured in Dulbecco's Modified Eagle Medium (PM150210, Procell) supplemented with 5% Fetal

Bovine Serum (164210, Procell). Cells were maintained in a CO_2 incubator at 37℃. Once cultures reached 70%–80% confluency, they were serum-starved for 12 hours and then randomly assigned to the following treatment groups: CTR, LPS, LPS + TBHQ, LPS + GA-n, LPS + GA-C2, LPS + GA-n + ML385, and LPS + GA-C2 + ML385.

In the LPS treatment protocol, NRK-52E cells were subjected to 1 μg/mL LPS for a duration of 24 hours. Subsequently, the cells underwent treatment with cycloheximide (CHX, HY-12320, MedChemExpress) at a concentration of 20 μg/mL for specified time intervals (0, 2, 4, 8, 12, and 24 hours) following transfection with NEU1 small interfering RNA (siRNA).

2.6. Cell viability assay

Cover slips and cell counting plates were sterilized using 75% ethanol. A cell suspension was subsequently prepared and seeded into plates at a density of 5×10^3 cells per well, followed by an overnight incubation. Triplicate wells were established for each experimental treatment group. To assess the impact of varying concentrations of gibberellic acids (GA-A, GA-B, GA-C2, and GA-n) on the viability of NRK-52E cells, a series of gradient concentrations (0, 1, 5, 25, 50, 100, and 200 μg/mL) were administered and incubated for a duration of 24 hours.

For the assessment of GAs and Fer-1 on LPS and erastin (Era, HY-15763, MedChemExpress)-induced reduction in cell viability, cells were treated with gradient concentrations (1, 5, 25 μg/mL) of GA-A, GA-B, GA-C2, GA-n, or Fer-1 (5 μmol/L), followed by LPS (1 μg/mL) or Era (1 μmol/L) treatment. Following a 4-hour incubation period with 10 μL of 3-(4,5-dimethylthiazol-2-yl)-2,5-diphenyl tetrazolium bromide (MTT) solution, the culture medium was removed. Subsequently, 100 μL of DMSO was introduced into each well. Absorbance readings were then taken at a wavelength of 490 nm utilizing a microplate reader (Bio-Rad, iMark). Each measurement was conducted in triplicate to ensure reproducibility.

2.7. Histological evaluation

To assess the effects of GAs treatment on kidney function, we examined tissue damage in the kidneys. Following a previously established protocol [31–33], kidney tissue samples were fixed in paraformaldehyde for 24 hours. Subsequent to initial processing, the samples were subjected to a sequential treatment with graded ethanol concentrations and xylene to achieve further fixation. Post-embedding in paraffin wax, the tissues were sectioned into slices of 5 micrometers in thickness. These sections underwent a dewaxing process and were rehydrated through a gradient of ethanol, followed by a rinse with distilled water. Hematoxylin and eosin (HE) staining was conducted in accordance with the manufacturer's protocol (G1100, Solarbio).

To evaluate renal fibrosis, supplementary staining procedures were conducted utilizing Masson's trichrome (G1340, Solarbio) and Sirius Red (G1472, Solarbio) staining kits. The stained tissue sections were subsequently examined and imaged using a Nikon Eclipse E100 microscope (Nikon DS-U3, Japan). Quantitative assessment of renal fibrosis was carried out using ImageJ software.

2.8. Quantification of blood creatinine (Bcr) and blood urea nitrogen (BUN)

Plasma levels of blood creatinine were quantified utilizing a commercial assay kit (C011-2-1, NJJC Bio). Similarly, blood urea nitrogen levels were determined employing a urea nitrogen assay kit (C013-2-1, NJJC Bio).

2.9. Enzyme-linked immunosorbent assay (ELISA)

The concentrations of interleukin-1β (IL-1β), tumor necrosis factor-α (TNF-α), and neutrophil gelatinase-associated lipocalin (NGAL) were measured using specific ELISA kits: the mouse IL-1β ELISA kit (ml098416, mlbio), the mouse TNF-α kit (ml002095, mlbio), and the mouse NGAL ELISA kit (ml002141, mlbio). These measurements were performed with an enzyme labeling analyzer (Rayto RT-6100) following the protocols provided by the manufacturer.

2.10. Western blot analysis

Kidney tissues were lysed with RIPA buffer (R0010, Solarbio) containing PMSF (P0100, Solarbio) at a 100:1 ratio, followed by ultrasonic treatment. After centrifugation, protein concentrations were determined using the bicinchoninic acid method (C503021-0500, Sangon Biotech). Protein samples were subjected to separation via SDS-PAGE and subsequently transferred onto a nitrocellulose membrane. After a blocking step, the membrane was incubated overnight at 4℃ with primary antibodies, including prostaglandin-endoperoxide synthase 2 (PTGS2, 27308-1-AP, Proteintech, 1:1000), inducible nitric oxide synthase (iNOS, #2982, CST, 1:1000), transforming growth factor-β1 (TGF-β1, ab31013, Abcam, 1:1000), NF-κB p65 (YM8209, Immunoway, 1:1000), phosphorylated nuclear factor-κB p65 (Ser536) (p-NF-κB, YP0191, Immunoway, 1:1000), inhibitor of nuclear factor kappa B α (IκBα, #4812, CST, 1:1000), Akt (GB15689, Servicebio, 1:1000), phosphorylated protein kinase B (p-Akt, GB150002, Servicebio, 1:1000), GSK3β (GB11099, Servicebio, 1:1000), phosphorylated glycogen synthase kinase 3β (p-GSK3β, GB114582, Servicebio, 1:600), Nrf2 (sc-365949, Santa Cruz Biotechnology, 1:1000), Keap-1 (sc-514914, Santa Cruz Biotechnology, 1:1000), heme oxygenase-1 (HO-1, sc-390991, Santa Cruz Biotechnology, 1:1000), solute carrier family 7 member 11 (SLC7A11, #98051, CST, 1:1000), FSP1 (sc-377120, Santa Cruz Biotechnology, 1:1000), and GPX4 (sc-166570, Santa Cruz Biotechnology, 1:1000). The subsequent day, following the removal of the primary antibody, the membrane was incubated with a goat anti-rabbit secondary antibody (SE134, Solarbio) at a dilution of 1:5000. Actin expression served as a loading control and was detected using a β-actin antibody (GB15001, Servicebio) at a dilution of 1:3000, along with an HRP-conjugated goat anti-mouse secondary antibody (SE131, Solarbio) at a dilution of 1:5000. Immunoreactive bands were visualized utilizing the e-BLOT ECL system (China), and the intensity of the protein bands was quantified using Image-Pro Plus 6.0 software.

2.11. Quantitative reverse transcription-polymerase chain reaction (qRT-PCR)

Total RNA was isolated from NRK-52E cells utilizing the Trizol reagent, followed by complementary DNA synthesis employing the Reverse Transcription Kit from Toyobo. The primers, as specified in Table 1, were synthesized by Shanghai Sangon. qRT-PCR was conducted using the SYBR Green Master Mix and

primers at a concentration of 1 M. Gene expression levels were normalized to glyceraldehyde-3-phosphate dehydrogenase (GAPDH) as the reference gene.

Table 1. qRT-PCR primer sequences.

Gene	Sequence (5′ → 3′)
TNF-α	(F) AAGCCCGTAGCCCACGTCGTA
	(R) GCCCGCAATCCAGGCCACTAC
IL-1β	(F) CCAGGATGAGGACCCAAGCA
	(R) TCCCGACCATTGCTGTTTCC
Nrf2	(F) TTGTAGATGACCATGAGTCGC
	(R) CAGGGGTGGTGAAGACTGAG
HO-1	(F) CCTTCCCGAACATCGACAGCC
	(R) GCAGCTCCTCAAACAGCTCAA
SLC7A11	(F) GGCATGAGAAGGTGGTTCTG
	(R) CTGCCCGTGTTCTGGAGTAT
GPX4	(F) AATTCGCAGCCAAGGACATC
	(R) GGCCAGGATTCGTAAACCAC
FSP1	(F) GGCAAAGTGATTGGCATAGA
	(R) TGGATCTGCTTCACCATGTC
NEU1	(F) TTCATCGCTATGAGGAGGTCCA
	(R) GAAGGGAATGCCGCTCACTCCA
GAPDH	(F) CAAGGCTGAGAATGGGAAGC
	(R) GAAGACGCCAGTAGACTCCA

2.12. Detection of malondialdehyde (MDA), hydrogen peroxide (H2O2), superoxide dismutase (SOD), and GSH levels in cell and kidney tissue samples

The activity of MDA (D799761-0050, Sangon Biotech), H_2O_2 (BC3595, Solarbio), SOD (D799593-0050, Sangon Biotech), and GSH (A006-2-1, NJJC Bio) was measured using specific commercial assay kits.

2.13. Iron measurements

The Ferrous Ion Content Assay Kit (BC5410, Solarbio) was used to quantify the Fe^{2+} content in the samples. The analysis was performed following the manufacturer's protocol.

2.14. Network pharmacological analysis

To elucidate target proteins linked to the medicinal constituents of GAs and gene targets pertinent to sepsis, we employed the Super-PRED database (https://prediction.charite.de/) alongside the DisGeNET database (https://disgenet.com/). Official human genetic nomenclature was sourced from the UniProt database (https://www.uniprot.org/). The principal targets of GAs were juxtaposed with disease-associated genes utilizing the Venny 2.1.0 tool (https://bioinfogp.cnb.csic.es/tools/venny). Construction of the protein-protein interaction (PPI) network was conducted using the STRING database (https://cn.string-db.org/), with visualization facilitated by Cytoscape 3.9.0. The identified targets underwent Gene Ontology (GO) and Kyoto Encyclopedia of Genes and Genomes (KEGG) pathway enrichment analysis via the DAVID database (https://david.ncifcrf.gov/summary.jsp). A stringent p-value threshold of less than 0.05 was applied to discern significant cellular components, molecular functions, biological processes, and signaling pathways associated with these targets.

2.15. Molecular docking

Molecular docking analysis of GA-C2 and Zanamivir with NEU1 (PDB ID: 8DU5) was performed using PyMOL and AutoDock Tools. The minimum binding energies for the target compounds and their components were calculated using AutoDock Vina. The docking results were visualized using PyMOL.

2.16. Immunohistochemistry

The collected kidney tissue samples were processed for immunohistochemical staining. Kidney sections were dewaxed, peroxidase activity was quenched, and blocking with serum was performed for 30 minutes. A primary antibody was applied to the sections and incubated overnight at 4℃. Subsequently, a secondary antibody was introduced, and the sections were subjected to three washes with phosphate-buffered saline (PBS, PB180327, Procell). A 3,3'-Diaminobenzidine chromogen solution (DA1016, Solarbio) was then applied, with color development being carefully monitored and controlled using a microscope. Positive staining was indicated by a brownish-yellow coloration. Upon achieving the desired staining intensity, the color development process was halted. The sections underwent counterstaining with a nuclear stain, followed by dehydration. Finally, the sections were examined under a microscope for image acquisition and subsequent analysis.

2.17. Fluorescent probes to observe reactive oxygen species (ROS) levels

Fluorescent probes were employed to quantify ROS levels in NRK-52E cells cultured on a sterile coverslip. Post-treatment, the coverslip was removed, excess medium was absorbed, and 100 μL of 2′,7′-Dichlorodihydrofluorescein Diacetate (DCFH-DA, D6470, Solarbio) probe solution was applied. The slide was gently agitated to ensure uniform coverage of the cells and subsequently incubated for 30 minutes. Following incubation, the dye was aspirated, and the cells were washed three times with medium, each wash lasting 5 minutes. Finally, the cells were examined using a fluorescence microscope.

2.18. siRNA transfection protocol

In this study, siRNA was employed to silence endogenous NEU1, thereby achieving targeted RNA interference. The siRNA transfection procedure was performed as previously described [34]. Briefly, NRK-52E cells were seeded in six-well plates and cultured until reaching 70%–80% confluence. Transfections were carried out using either NEU1-specific siRNA or a negative control (NC) siRNA (both obtained from Bioneer) with the HiPerFect transfection reagent (Qiagen) for 24 hours. Following the initial transfection period, the medium containing residual siRNA was removed and replaced with fresh medium supplemented with LPS, which was then incubated for an additional 24 hours. Cells were harvested at 48 hours post-transfection for subsequent RNA extraction and qPCR analysis. For Western blot assays, after the initial 24-hour siRNA transfection, the medium was replaced with standard growth medium, and cells were cultured for another 24 hours before LPS treatment. LPS was then added, and incubation continued for an additional 24 hours prior to cell collection. To ensure rigorous experimental controls, a NC siRNA + LPS group was included in the design to exclude nonspecific effects arising from siRNA transfection or LPS stimulation alone.

2.19. Co-immunoprecipitation (Co-IP)

The cells underwent two washes with pre-chilled PBS, ensuring the complete removal of PBS after the final wash. Subsequently, pre-chilled radioimmunoprecipitation assay buffer was added to lyse the cells, and the lysate was subjected to centrifugation at 14,000 g for 15 minutes at 4℃ to collect the supernatant. The supernatant was then incubated with primary antibodies (NEU1, 67032-1-Ig, Proteintech, 1:100; Keap-1, 10503-2-AP, Proteintech, 1:600) overnight at 4℃. Following incubation, the samples were combined with 100 μL of pre-treated protein A/G magnetic beads (P2179, Beyotime Biotechnology) and incubated on a shaking platform at 4℃ for one hour. Magnetic separation was performed, and the supernatant was discarded. The immunoprecipitated complex was washed five times with a pre-cooled lysate buffer devoid of protease inhibitors (P0100, Solarbio) to eliminate unbound proteins. Subsequently, loading buffer (LT101, EpiZyme) was added to the samples, which were then boiled at 100℃ for five minutes. Western blotting analysis was subsequently conducted to detect the corresponding samples.

2.20. Cellular thermal shift assay (CETSA)

NRK-52E cells were exposed to GA-C2 at a concentration of 25 μg/mL or to DMSO (catalog number D8371, Solarbio) for a duration of 24 hours. Post-treatment, the cells were harvested and distributed into eight PCR tubes (catalog number 403022, NEST Biotechnology). These aliquots were subjected to a range of temperatures from 40℃ to 75℃ for three minutes using a thermal cycler (Eppendorf, Germany). Subsequently, the samples were allowed to return to ambient temperature and underwent three freeze-thaw cycles utilizing liquid nitrogen. The supernatant was then isolated by centrifugation at 4℃ at 12,000 g for 20 minutes and subsequently analyzed via Western blotting to evaluate the thermal stability of the proteins.

2.21. Data analysis

The experimental results were analyzed statistically utilizing GraphPad Prism version 9.4. Each experiment was conducted in triplicate, and the data are presented as the mean ± standard error of the mean (SEM). Tests for normality and lognormality were conducted to verify that the data conformed to a normal distribution. Differences among multiple groups were assessed using a one-way analysis of variance, followed by Tukey's post hoc test. *P*-value of less than 0.05 was considered indicative of statistical significance, with significance levels classified as follows: $P < 0.05$, $P < 0.01$, and $P < 0.001$.

3. Results

3.1. Rapid separation of GAs from Ganoderma lucidum by-products

The structures of GA-A, GA-B, and GA-C2 are illustrated in Fig. 1A. To effectively separate the GAs from *Ganoderma lucidum* by-products, we employed flash medium-pressure preparative liquid chromatography (Fig. 1B), followed by high-pressure preparative chromatography (Fig. 1C). This sequential separation process successfully resolved GA-enriched fractions. Mixture 1 primarily consisted of GA-C2 with a purity of 98%, while Mixture 2 contained GA-A and GA-B with minimal contamination of GA-C2. Mixture 3 contained unresolved GAs, including Ganoderic acid D, enoic acid D, C1, and H, requiring additional

purification steps. Through high-performance liquid chromatography (HPLC) analysis, the purities of isolated GA-A, GA-B, and GA-C2 were confirmed to be more than 98% (Fig. 1D).

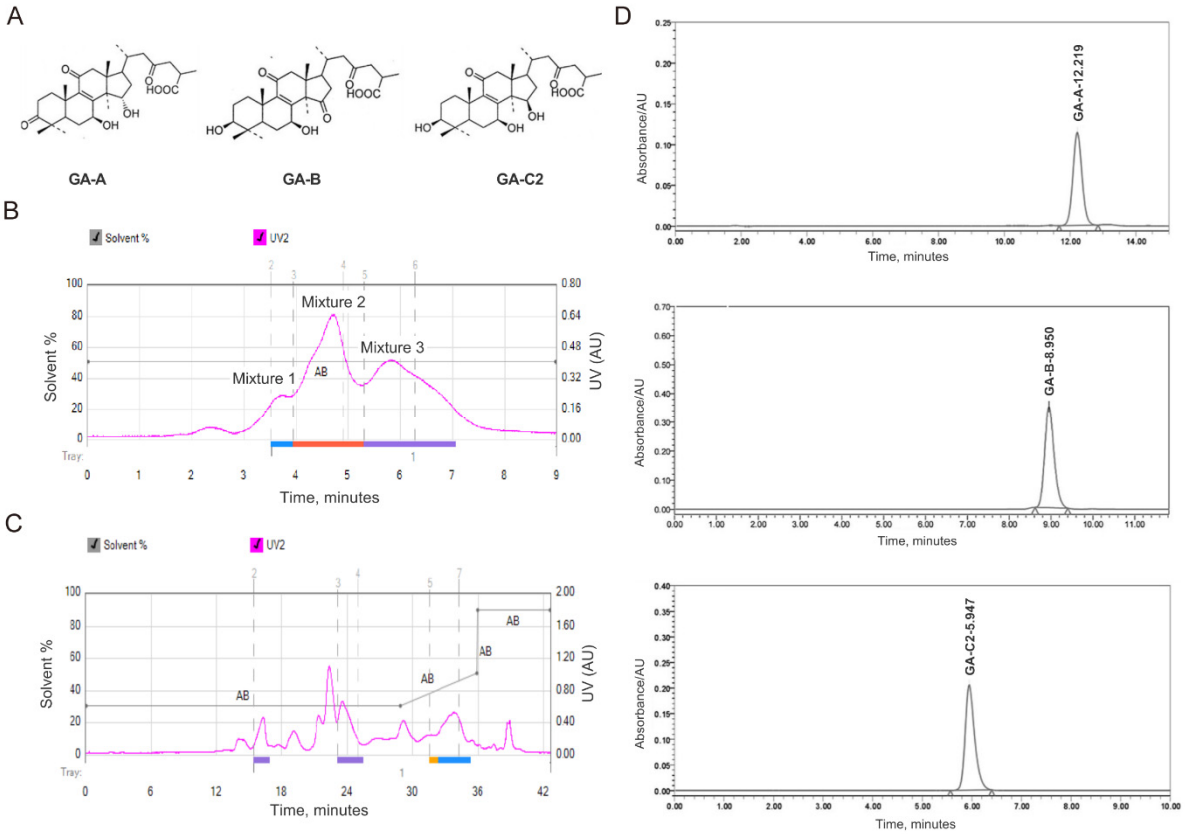

Fig. 1. Determination, separation, and purification of GAs. (A) Structural identification of GA-A, GA-B and GA-C2. (B) Flash chromatography profile demonstrating the separation of GA-A, GA-B and GA-C2. (C) High-pressure preparative chromatography profile showing the separation of GA-A, GA-B and GA-C2. (D) HPLC purity chromatograms of GA-A, GA-B and GA-C2.

3.2. Ferroptosis inhibition attenuates LPS-induced AKI

To examine the role of ferroptosis in LPS-induced AKI, C57BL/6 mice were pre-treated with the ferroptosis inhibitor Fer-1 one hour prior to LPS administration, followed by LPS injection 24 hours before euthanasia (refer to Fig. 2A). Western blot analysis demonstrated that LPS treatment resulted in a significant 113% increase in PTGS2 expression, while simultaneously causing a reduction in the expression of key anti-ferroptotic markers: SLC7A11 by 66%, GPX4 by 72%, and FSP1 by 69%. Treatment with Fer-1 reversed these changes (Fig. 2B). In comparison to the LPS-only group, Fer-1 treatment restored GSH levels to 2.76 times that of LPS-treated mice and reduced renal iron content by 31% (Fig. 2C, D). Additionally, Fer-1 treatment resulted in a 37% reduction in serum TNF-α levels and a 25% reduction in IL-1β levels (Fig. 2E, F). LPS-induced increases in renal MDA by 34% and decreases in SOD by 51% were normalized by Fer-1 treatment (Fig. 2G, H). Histopathological analysis revealed that Fer-1 alleviated LPS-induced tubular injury, characterized by vacuolization, brush border loss, and casts in the renal cortex (Fig. 2I). Moreover, Masson's trichrome staining revealed an elevation in renal fibrosis in mice treated with LPS compared to the control group, an effect that was mitigated by Fer-1 treatment (Fig. 2J). This finding was corroborated by Picrosirius red staining, which demonstrated a reduction in cortical collagen deposition following Fer-1 administration

(Fig. 2K). These results suggest that the protective effect of Fer-1 against LPS-induced AKI is linked to the inhibition of ferroptosis.

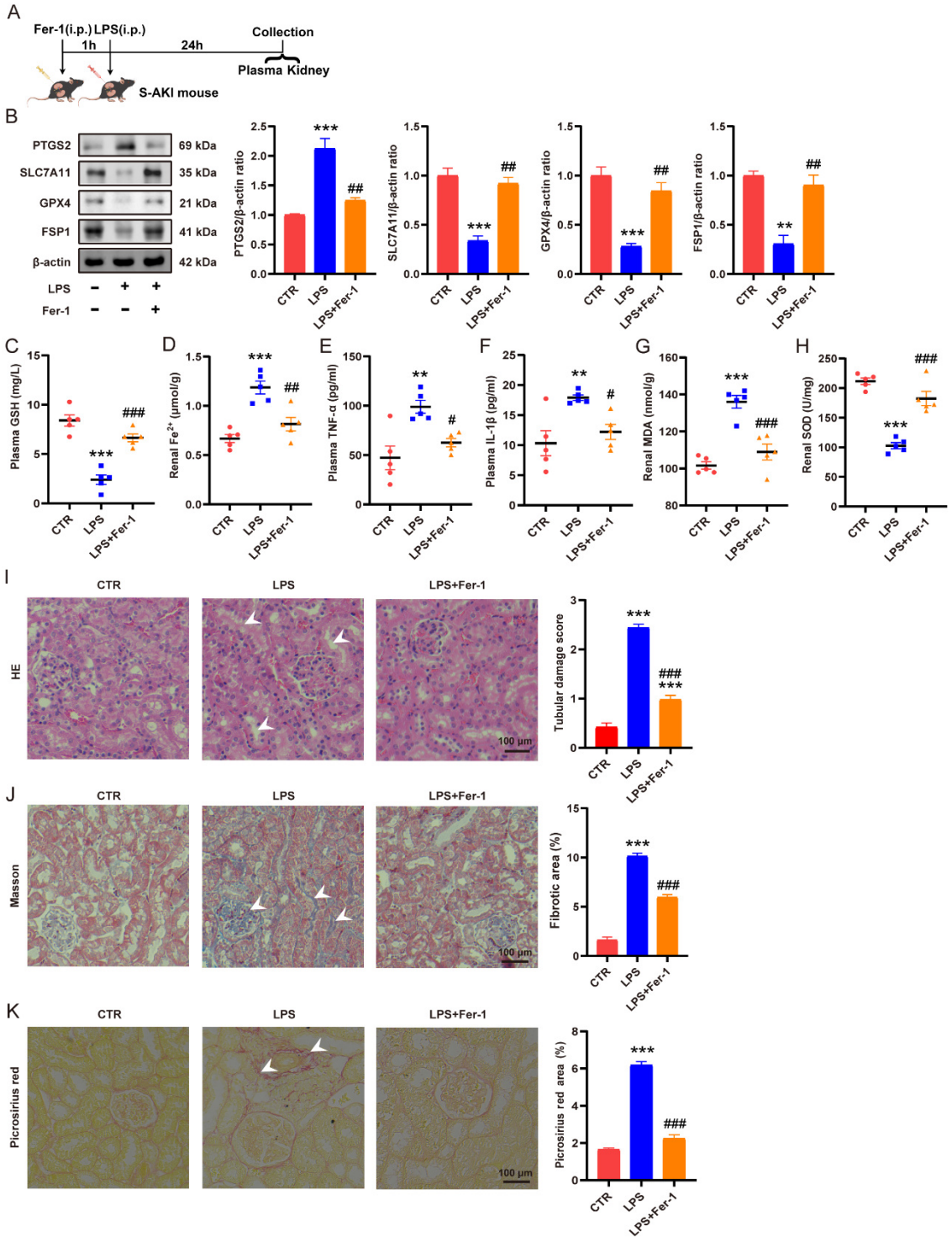

Fig. 2. Ferroptosis inhibition mitigates LPS-induced kidney injury in mice. (A) Experimental procedure. (B) Representative Western blots of PTGS2, SLC7A11, GPX4, and FSP1, along with their relative expression levels (n=3). (C) Plasma GSH levels (n=5). (D) Renal Fe^{2+} levels (n=5). (E) Plasma TNF-α levels (n=5). (F) Plasma IL-1β levels (n=5). (G) Renal MDA levels (n=5). (H) Renal SOD levels (n=5). (I) Representative images of HE staining of the renal cortex. Arrows indicate renal tubular dilatation, vacuolization, and focal proteinaceous casts in tubular cells. Tubular injury is assessed by identifying renal tubules exhibiting injury signs (n=5). Scale bar: 100 μm. (J) Illustrations of typical Masson's trichrome staining (injury appears blue) and morphometric analysis of Masson-stained kidney slices (n=3). Scale bar: 100 μm. (K) Identification of injury areas via Sirius red staining (collagen appears red); the ratio of Sirius red-stained injury area to total area is used to quantify the value (n=6). Scale bar: 100 μm. Data are presented as mean ± SEM. Statistical significance is indicated as $^{*}P < 0.05$, $^{**}P < 0.01$, and $^{***}P < 0.001$ versus the CTR group, and $^{\#}P < 0.05$, $^{\#\#}P < 0.01$, and $^{\#\#\#}P < 0.001$ versus the LPS group.

3.3. GAs ameliorate renal dysfunction in LPS-induced septic AKI

In the study, mice with LPS-induced septic AKI were administered daily intraperitoneal injections of GA-A, GA-B, GA-C2, GA-n-L, or GA-n-H for three days as a pre-treatment (Fig. 3A). GA-n-H and GA-C2 demonstrated notable reductions in serum biomarkers compared to the LPS group, including Bcr (47% and 49%), BUN (49% and 49%), and NGAL (60% and 48%) (Fig. 3B-D). Kidney tissues were evaluated using HE, Masson's, and Picrosirius red staining. The LPS group exhibited tubular damage characterized by vacuolization, renal tubular dilatation, and tubular casts in HE staining. Additionally, Masson's staining revealed a significantly larger fibrotic area, and increased Picrosirius red staining was observed in the cortical region. Treatment with GA-n-H and GA-C2 significantly mitigated these alterations (Fig. 3E-H). These findings demonstrate the effective alleviation of LPS-induced renal dysfunction in septic AKI mice by GA-n, particularly GA-C2.

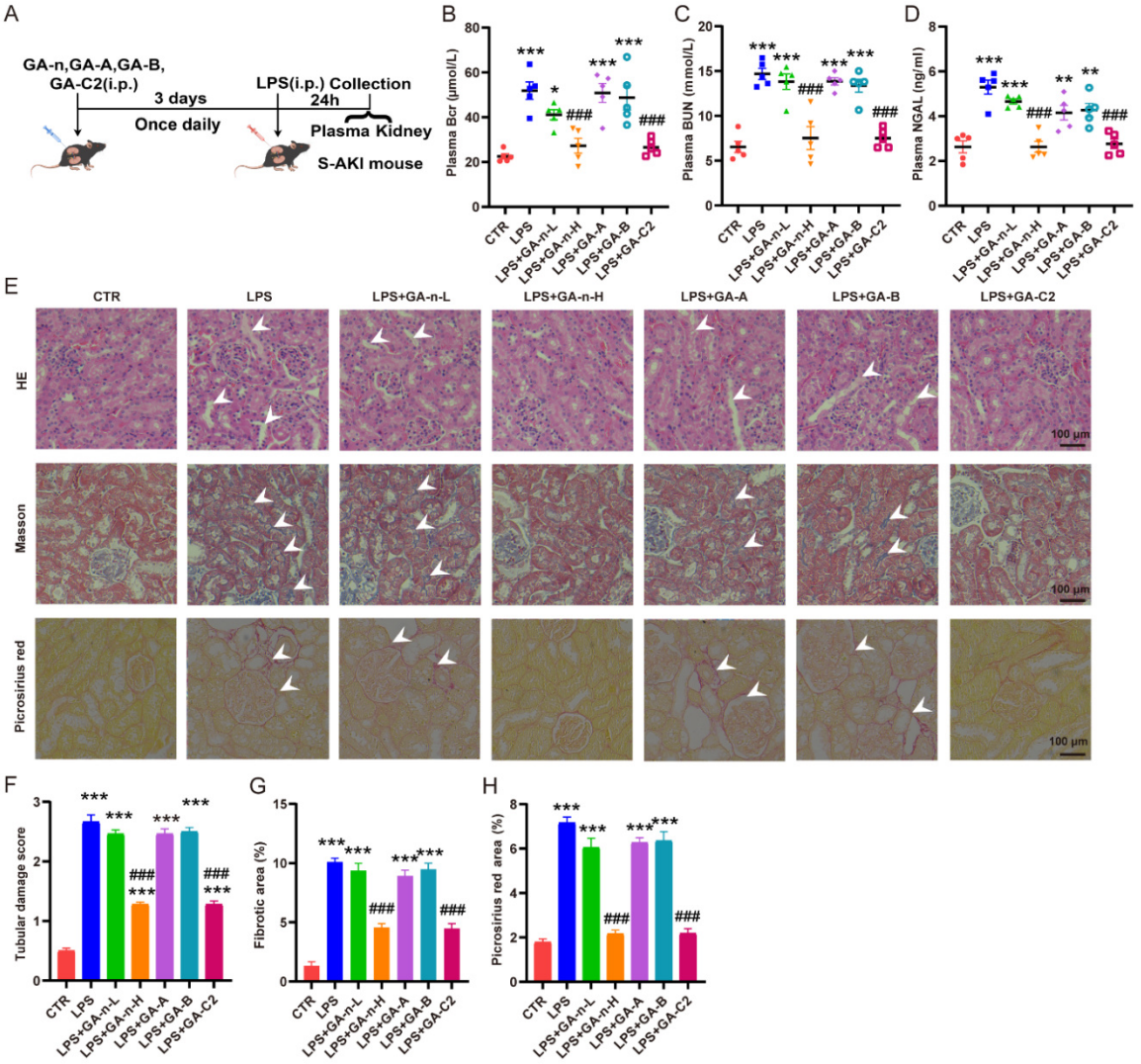

Fig. 3. Protective effects of GAs on LPS-induced renal injury in mice. (A) Experimental procedure. (B) Plasma Bcr levels (n=5). (C) Plasma BUN levels (n=5). (D) Plasma NGAL levels (n=5). (E) Representative images of HE staining of the renal cortex. Arrows indicate renal tubular dilatation, vacuolization, and focal proteinaceous casts in tubular cells. Scale bar: 100 μm. Illustrations of typical Masson's trichrome staining (injury appears blue), Scale bar: 100 μm. Identification of injury areas via Sirius red staining (collagen appears red). Scale bar: 100 μm. (F) Tubular injury assessment is performed by identifying renal tubules exhibiting injury signs (n=5). (G) Morphometric analysis of Masson-stained kidney slices (n=3). (H) Identification of injury areas via Sirius red staining, the ratio of Sirius red-stained injury area to total area is used to quantify the value (n=6). Data are shown as mean ± SEM. Statistical significance is indicated as $^{*}P < 0.05$, $^{**}P < 0.01$, and $^{***}P < 0.001$ versus the CTR group, and $^{\#}P < 0.05$, $^{\#\#}P < 0.01$, and $^{\#\#\#}P < 0.001$ versus the LPS group.

3.4. GAs attenuate oxidative stress, ferroptosis, and inflammation in S-AKI mice

To evaluate the effects of GAs on LPS-induced renal oxidative stress, we quantified MDA and SOD levels. LPS administration resulted in a 49% elevation in renal MDA levels compared to the control group. However, treatment with GA-n-H and GA-C2 significantly reduced MDA levels by 49% and 54%, respectively (Fig. 4A). Furthermore, SOD activity, which decreased by 50% in LPS-treated mice, was restored to baseline levels following administration of GA-n-H and GA-C2 (Fig. 4B). In this murine model, GA-n-H and GA-C2 markedly reduced the concentrations of pro-inflammatory cytokines, including TNF-α by 29% and 34%, and interleukin-1 beta (IL-1β) by 26% and 25%, relative to LPS treatment alone (Fig. 4C and 4D). Additionally, GA-n-H and GA-C2 effectively inhibited the activation of iNOS and TGF-β1 proteins in the kidneys, resulting in a reduction of iNOS levels by 57% and 50%, and TGF-β1 by 50% (Fig. 4E). Moreover, these treatments decreased the p-NF-κB by 54% and 55%, while enhancing the levels of IκBα by 2.61-fold and 2.75-fold, thereby restoring them to normal levels. There were no significant differences in total NF-κB protein levels among the groups (Fig. 4F). Immunohistochemical analysis of NF-κB phosphorylation corroborated these results, demonstrating a reduction in brown-positive areas in kidney sections treated with GA-n-H and GA-C2 relative to the LPS group (Fig. 4G).

Western blot analysis was performed on kidney tissue to assess the expression levels of ferroptosis-associated proteins, including PTGS2, SLC7A11, GPX4, and FSP1. In comparison to the CTR group, the LPS group demonstrated a 138% increase in PTGS2 levels, alongside reductions in SLC7A11, GPX4, and FSP1 levels by 44%, 55%, and 42%, respectively. Notably, administration of GA-n-H and GA-C2 resulted in a significant reduction in PTGS2 levels and an elevation in SLC7A11, GPX4, and FSP1 protein levels. Conversely, treatments with GA-n-L, GA-A, and GA-B did not produce significant alterations in the levels of these ferroptosis-related proteins (refer to Fig. 4H).

Moreover, compared to the LPS group, GA-n-H and GA-C2 administration significantly increased the levels of reduced GSH by 2.38 times and 2.32 times, respectively (Fig. 4I), and decreased ferric ion concentrations by 55% and 54% (Fig. 4J). Treatment with GA-n-L, GA-A, and GA-B did not show noticeable effects on these parameters compared to the LPS group.

These results demonstrate that GA-n-H and GA-C2 provide protection against oxidative stress, ferroptosis, and inflammatory responses induced by LPS.

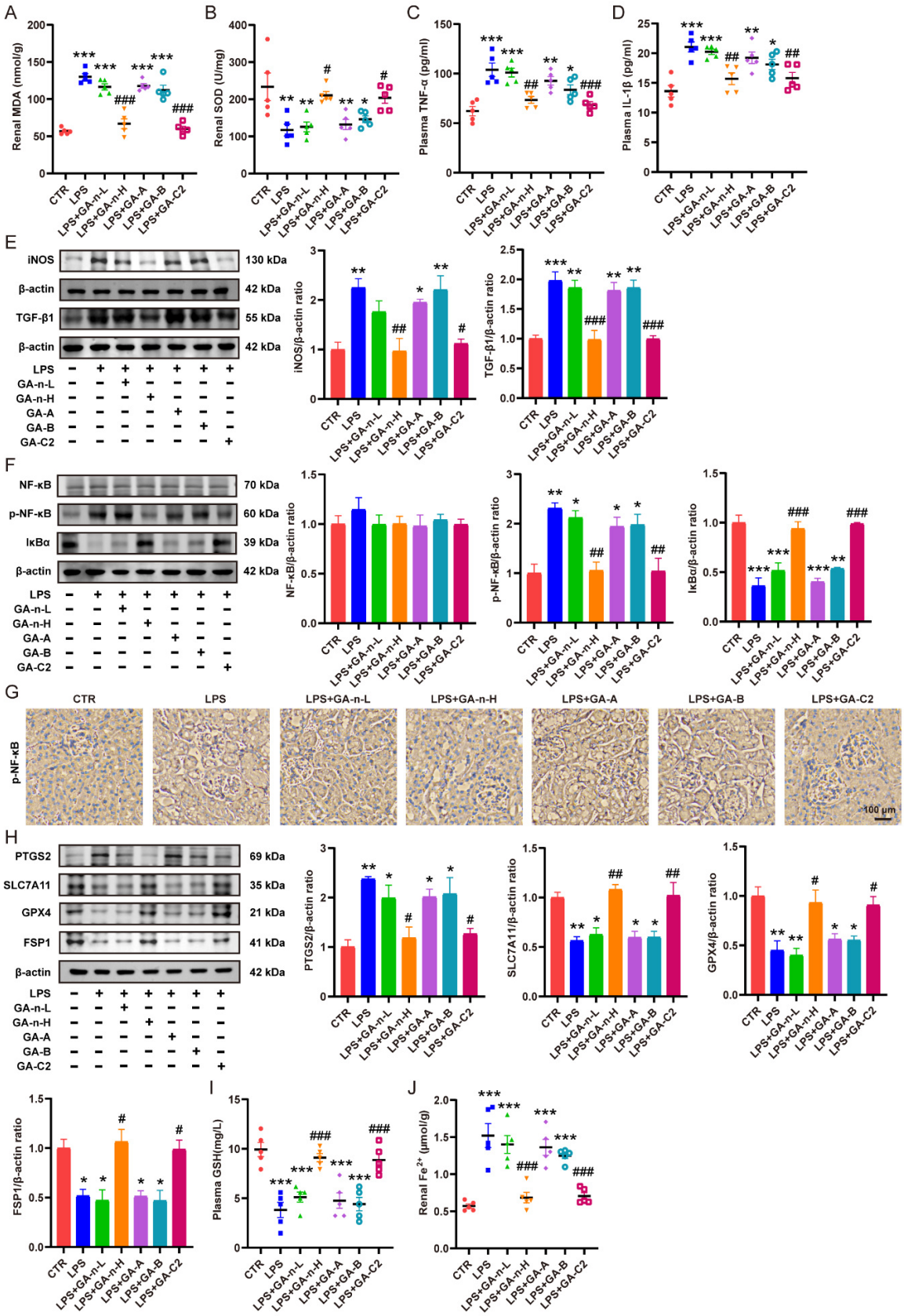

Fig. 4. GAs alleviate oxidative stress, inflammation, and ferroptosis in S-AKI Mice. (A) Renal MDA levels (n=5). (B) Renal SOD levels (n=5). (C) Plasma TNF-α levels (n=5). (D) Plasma IL-1β levels (n=5). (E) Representative Western blots of iNOS and TGF-β1, along with their relative expression levels (n=3). (F) Bands of NF-κB, p-NF-κB, and IκBα, along with their relative expression levels (n=3). (G) Representative images of p-NF-κB immunohistochemistry in kidney tissue. Scale bar: 100 μm. (H) Representative Western blots of PTGS2, SLC7A11, GPX4, and FSP1, along with their relative expression levels (n=3). (I) Plasma GSH levels (n=5). (J) Renal Fe^{2+} levels (n=5). Data are shown as mean ± SEM. Statistical significance is indicated as $^{*}P < 0.05$, $^{**}P < 0.01$, and $^{***}P < 0.001$ versus the CTR group, and $^{\#}P < 0.05$, $^{\#\#}P < 0.01$, and $^{\#\#\#}P < 0.001$ versus the LPS group.

3.5. Network pharmacological analysis identifies potential targets and signaling pathways for GA-A, GA-B, and GA-C2 in sepsis

To investigate the potential targets and signaling pathways associated with GA-A, GA-B, and GA-C2 in the context of sepsis, a comprehensive network pharmacological analysis was performed. We identified 169 targets for GAs from the Super-PRED database and collected 1543 sepsis-related disease targets from the DisGeNET database. By comparing the two, we identified a total of 62 overlapping targets (Fig. 5A). Using these overlapping targets, we constructed a PPI network, which revealed core targets such as TNF, IL6, NFKB1, and PTGS2 (Fig. 5B).

To gain deeper insights, we conducted Gene Ontology (GO) and Kyoto Encyclopedia of Genes and Genomes (KEGG) pathway enrichment analyses utilizing the DAVID database. The GO analysis identified 400 GO terms, comprising 283 related to biological processes, 41 associated with cellular components, and 76 pertaining to molecular functions. The top 10 enriched terms are illustrated in Fig. 5C. Furthermore, the KEGG pathway analysis indicated that GA-A, GA-B, and GA-C2 might exert their preventive and therapeutic effects via the reactive oxygen species signaling pathway, as depicted in Fig. 5D. These results, in conjunction with existing literature [35], prompted us to focus on the Keap-1/Nrf2/HO-1 signaling pathway.

To examine protein expression levels in kidney tissue, we conducted western blot analysis (Fig. 5E). The findings indicated that stimulation with LPS significantly elevated Keap-1 levels by 118%. In contrast, treatment with GA-n-H or GA-C2 effectively reduced Keap-1 levels. Additionally, LPS exposure resulted in a decrease in Nrf2 and HO-1 levels by 46% and 52%, respectively, within the kidney tissue. However, treatment with GA-n-H or GA-C2 reversed these reductions. Immunohistochemical analysis of Nrf2 substantiated these findings, demonstrating an augmentation in brown-positive regions within kidney sections treated with GA-n-H and GA-C2, in contrast to the LPS group (Fig. 5F). Conversely, treatments with GA-n-L, GA-A, and GA-B did not produce a comparable effect.These results indicate that in S-AKI mice, GAs stimulate the Keap-1/Nrf2 pathway, as supported by the network pharmacological analysis and experimental validation.

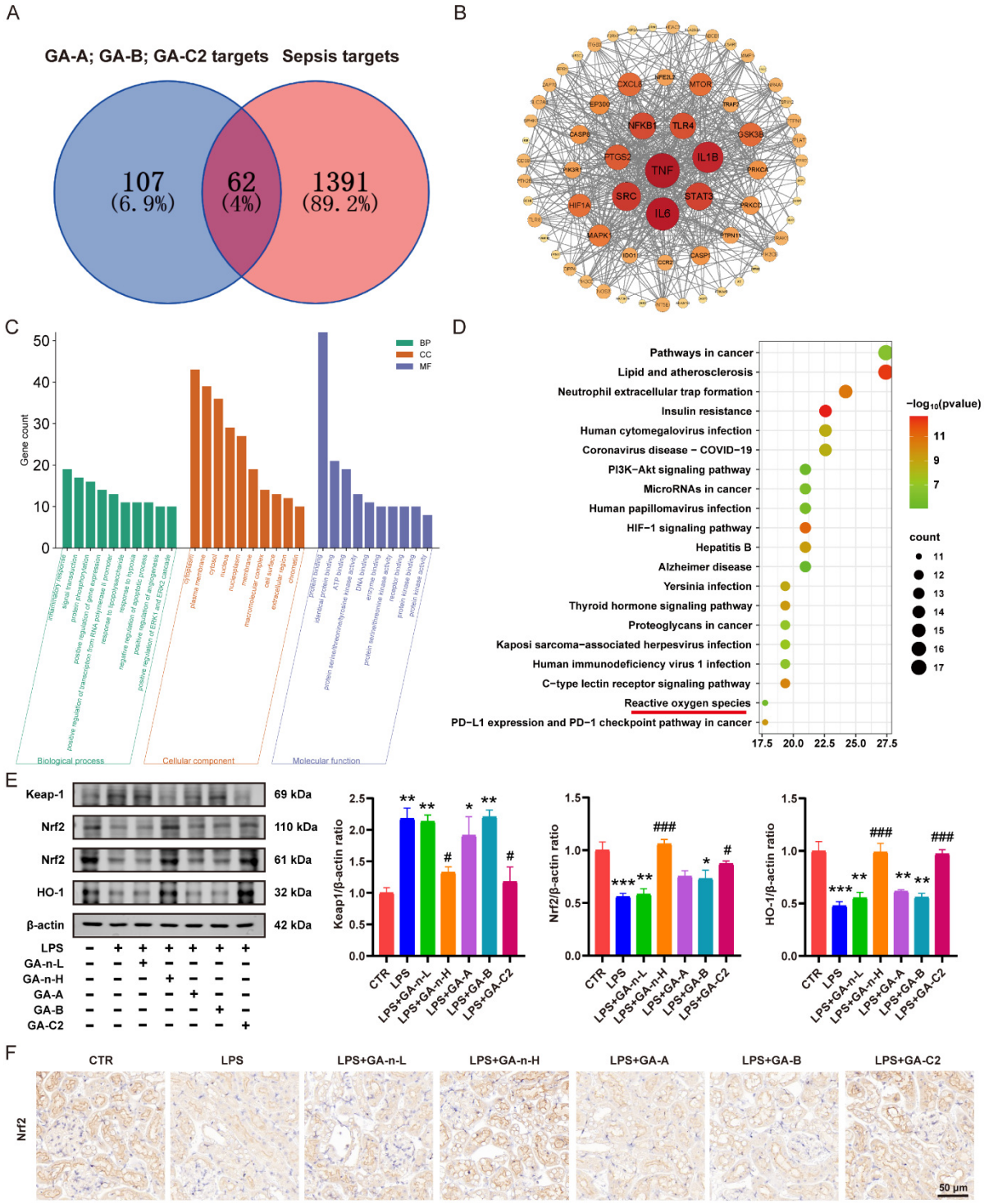

Fig. 5. Network pharmacology of GAs (GA-A, GA-B, and GA-C2) and their effect on the Keap-1/Nrf2 pathway in sepsis. (A) Venn diagram. (B) PPI network. (C) GO enrichment analysis. (D) KEGG pathway enrichment analysis. (E) Representative Western blots of Keap-1, Nrf2, and HO-1, along with their relative expression levels (n=3). (F) Representative images of Nrf2 immunohistochemistry in kidney tissue. Scale bar: 50 μm. Data are shown as mean ± SEM. Statistical significance is indicated as $^{*}P < 0.05$, $^{**}P < 0.01$, and $^{***}P < 0.001$ versus the CTR group, and $^{\#}P < 0.05$, $^{\#\#}P < 0.01$, and $^{\#\#\#}P < 0.001$ versus the LPS group.

3.6. GAs activate Nrf2 to inhibit ferroptosis in S-AKI mice

To examine the influence of GAs on the activation of the Nrf2 pathway and the inhibition of ferroptosis in mice with S-AKI, we developed a murine S-AKI model through LPS induction. The mice received intraperitoneal injections of GA-C2 or GA-n-H over a three-day period. For comparative purposes, TBHQ, a

known Nrf2 activator, was administered 8 hours prior to LPS administration, while ML385, an Nrf2 inhibitor, was administered 2 hours before LPS exposure (see Fig. 6A).

We quantified the protein levels of Nrf2 and HO-1 in renal tissue utilizing Western blot analysis (Fig. 6B). The data indicated that LPS stimulation resulted in a 60% reduction in Nrf2 expression and a 49% reduction in HO-1 expression. Conversely, treatment with TBHQ, GA-n-H, or GA-C2 led to an upregulation of Nrf2 and HO-1 expression. Notably, the co-administration of ML385 with GA-n-H or GA-C2 exerted a significant inhibitory effect on the expression of Nrf2 and HO-1. These findings were corroborated by immunohistochemical analysis of Nrf2, which revealed an increase in brown-positive areas in kidney sections treated with GA-n-H and GA-C2 compared to those treated with ML385 in combination with GA-n-H or GA-C2 (Fig. 6C).

In the murine model, TBHQ, GA-n-H, and GA-C2 significantly reduced pro-inflammatory cytokines TNF-α by 40%, 42%, and 47% (Fig. 6D) and IL-1β by 34%, 33%, and 36% (Fig. 6E) compared to LPS treatment alone. They also lowered MDA levels, an oxidative stress marker, by 46%, 38%, and 45% (Fig. 6F) and enhanced SOD activity, an antioxidant enzyme, by 66%, 75%, and 113% (Fig. 6G). However, ML385 negated the effects of GA-n-H and GA-C2.

Furthermore, we analyzed the protein expression of PTGS2, SLC7A11, GPX4, and FSP1 through Western blot analysis (Fig. 6H) to gain more insight into the mechanism of GAs. In comparison to the CTR group, the LPS group showed increased PTGS2 levels by 102% and decreased SLC7A11, GPX4, and FSP1 levels by 51%, 70%, and 60%, respectively. However, compared to LPS treatment alone, the addition of TBHQ, GA-n-H, and GA-C2 significantly reduced PTGS2 protein levels by 44%, 45%, and 45%, increased SLC7A11 by 98%, 102%, and 114%, GPX4 by 255%, 220%, and 241%, and FSP1 by 123%, 155%, and 120% protein expression in kidney tissue. Notably, this effect was abolished when ML385 was administered.

Moreover, compared to LPS treatment alone, the additional administration of TBHQ, GA-n-H, and GA-C2 significantly increased the levels of reduced GSH by 2.74 times, 2.61 times, and 3.00 times (Fig. 6I) and decreased ferric ion concentrations by 56%, 58%, and 45% (Fig. 6J). However, this protective effect was lost when ML385 was administered.

The results suggest that GA-n-H and GA-C2 trigger the Nrf2 pathway to prevent ferroptosis in S-AKI mice.

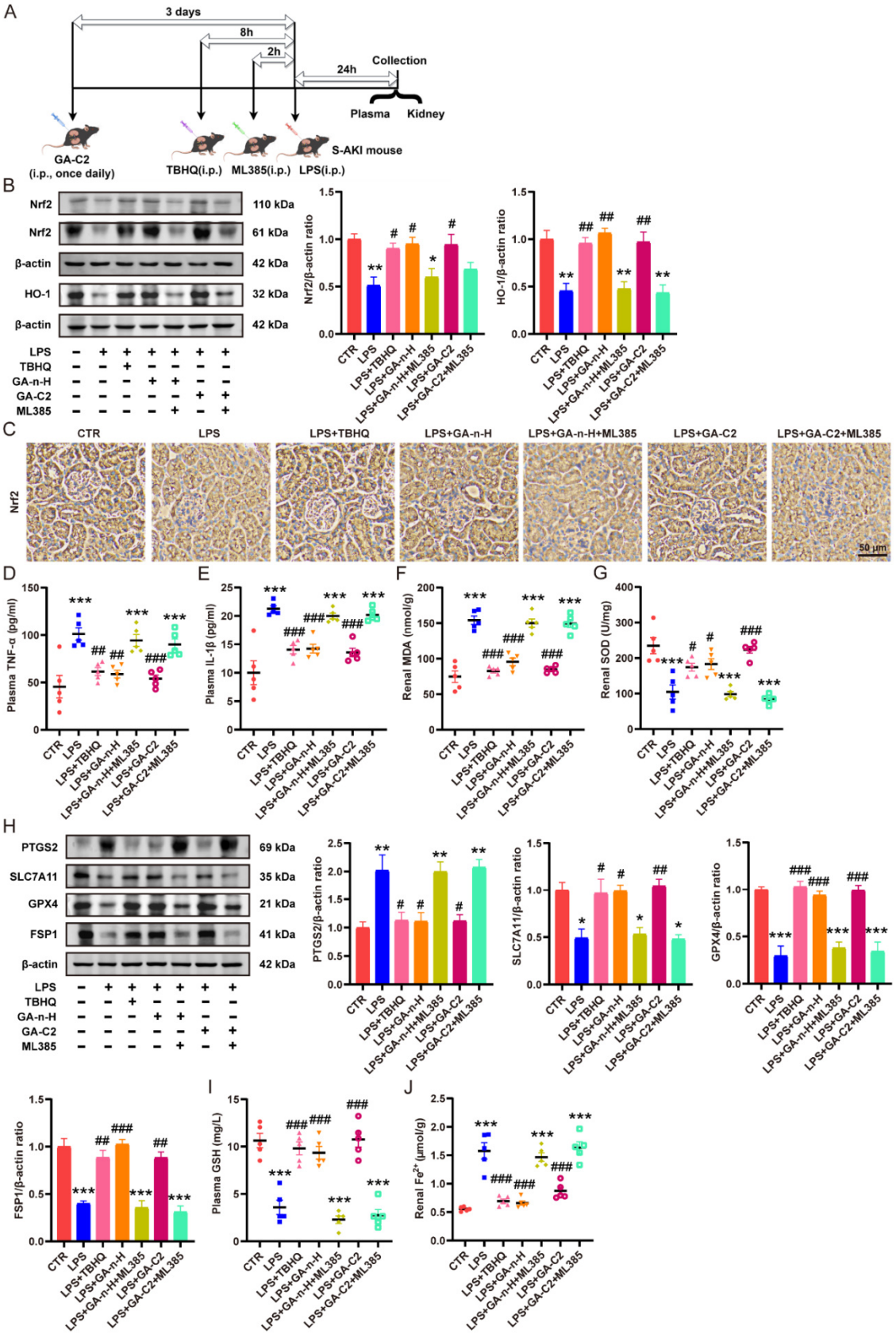

Fig. 6. GAs activate Nrf2 and protect against ferroptosis in S-AKI mice. (A) Experimental procedure. (B) Representative Western blots of Nrf2 and HO-1, along with their relative band densities (n=3). (C) Representative images of Nrf2 immunohistochemistry staining in renal tissues. Scale bar: 50 μm. (D) Plasma TNF-α levels (n=5). (E) Plasma IL-1β levels (n=5). (F) Renal MDA levels (n=5). (G) Renal SOD levels (n=5). (H) Representative Western blots of PTGS2, SLC7A11, GPX4, and FSP1, along with their relative expression levels (n=3). (I) Plasma GSH levels (n=5). (J) Renal Fe^{2+} levels (n=5). Data are shown as mean ± SEM. Statistical significance is indicated as $^{*}P < 0.05$, $^{**}P < 0.01$, and $^{***}P < 0.001$ versus the CTR group, and $^{\#}P < 0.05$, $^{\#\#}P < 0.01$, and $^{\#\#\#}P < 0.001$ versus the LPS group.

3.7. GAs alleviate LPS-induced NRK-52E cell damage by activating the Nrf2 pathway to inhibit ferroptosis

In this study, we examined the protective effects of GA-A, GA-B, GA-C2, and GA-n on LPS-induced damage in NRK-52E cells, focusing on the activation of the Nrf2 pathway to inhibit ferroptosis. NRK-52E cells were exposed to varying concentrations of GAs (1, 5, 25, 50, 100, 200 μg/ml) for a duration of 24 hours, and cell viability was evaluated using the MTT assay. The results indicated that different concentrations of GAs did not significantly affect cell viability (Fig. 7A). For practical purposes, a concentration of 25 μg/ml was selected for further investigation of GA-A, GA-B, GA-C2, and GA-n. The impact of these concentrations on LPS-damaged NRK-52E cells was assessed, revealing a marked reduction in cell viability following LPS stimulation. Nevertheless, treatment with 25 μg/ml of GA-C2 and GA-n notably improved the viability of NRK-52E cells compared to the LPS-treated group (Fig. 7B).

Furthermore, we investigated the role of GAs in inhibiting ferroptosis using Era-induced cell death as a model. Treatment with Era and the ferroptosis inhibitor Fer-1 demonstrated that Era induces ferroptosis in NRK-52E cells. Interestingly, GA-n and GA-C2 reversed the Era-induced decline in cell viability, indicating their role in inhibiting ferroptosis (Fig. 7C).

We further investigated the impact of GA-C2 and GA-n on the expression levels of TNF-α and IL-1β in NRK-52E cells. The administration of TBHQ, GA-n, and GA-C2 resulted in a significant reduction in both mRNA and protein levels of TNF-α and IL-1β when compared to the LPS-treated group. However, this inhibitory effect was negated upon the introduction of ML385, as illustrated in Fig. 7D-G.

In the LPS model group, levels of H_2O_2 increased by 60% and GSH decreased by 75%. Treatment with TBHQ, GA-n, and GA-C2 reversed these alterations. Additionally, DCFH-DA fluorescent probe staining revealed that ROS levels were significantly reduced by TBHQ, GA-n, and GA-C2 after LPS stimulation (Fig. 7H-J).

Western blot analysis revealed that LPS stimulation resulted in a reduction in the expression levels of Nrf2 by 53%, HO-1 by 58%, SLC7A11 by 44%, GPX4 by 70%, and FSP1 by 61%. Conversely, treatment with TBHQ, GA-n, or GA-C2 led to a significant upregulation of these proteins in kidney tissue (Fig. 7K). Similarly, the mRNA expression levels of Nrf2, HO-1, SLC7A11, GPX4, and FSP1 were diminished in the LPS model group but showed a marked increase following treatment with TBHQ, GA-n, and GA-C2. This protective effect was negated by the administration of ML385 (Fig. 7L-P).

These findings imply that GA-C2 and GA-n reduce LPS-induced damage in NRK-52E cells through the activation of the Nrf2 pathway, thereby inhibiting ferroptosis.

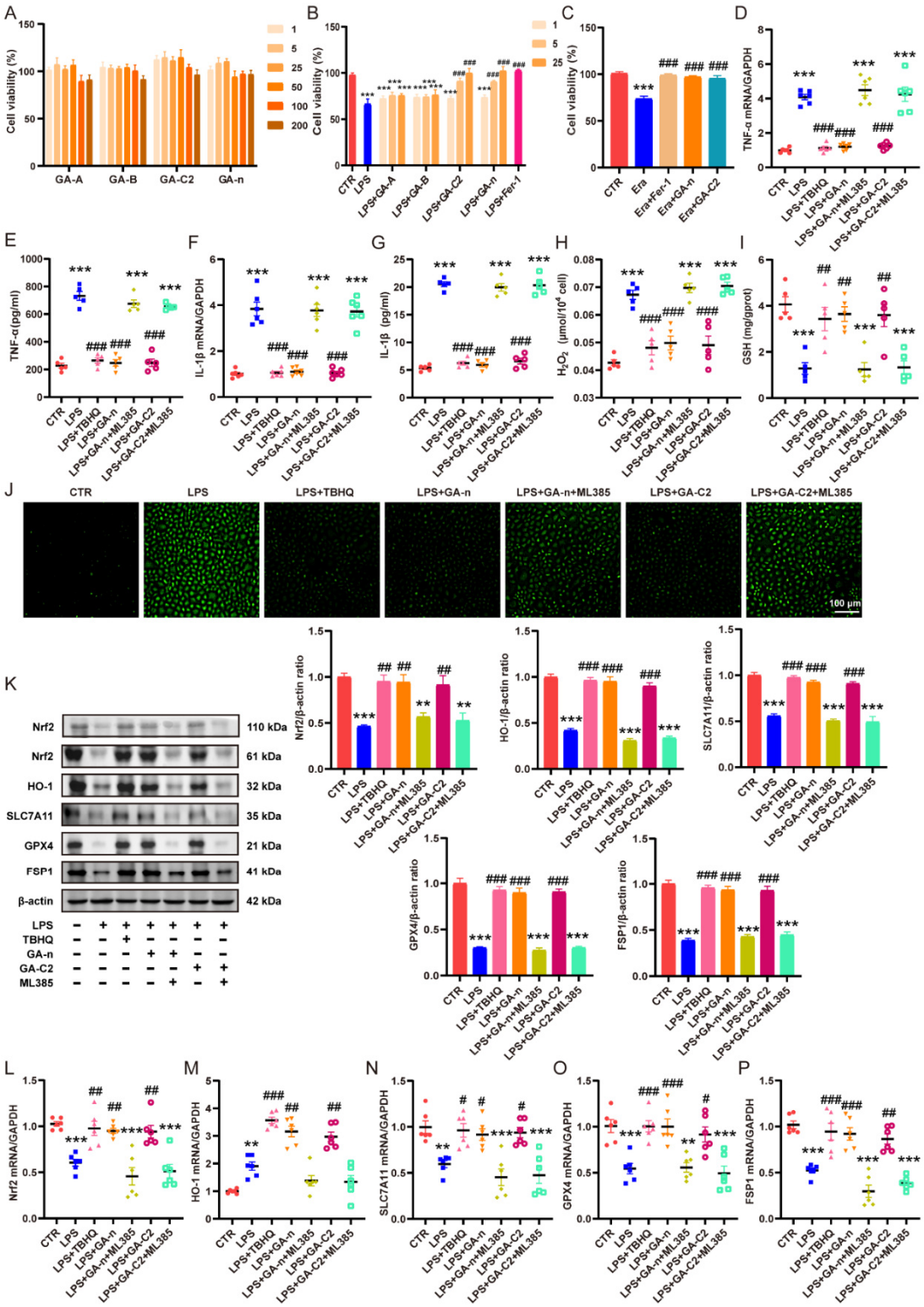

Fig. 7. GAs protect NRK-52E cells from LPS-induced damage by modulating Nrf2 and ferroptosis. (A) MTT assay determining the optimal concentration of GAs (n=5). (B) Effect of GAs on cell viability following LPS-induced damage in NRK-52E cells after 24 hours (n=5). (C) Effect of Fer-1, GA-n, and GA-C2 on cell viability following LPS-induced damage in NRK-52E cells after 24 hours (n=5). (D) qRT-PCR analysis of TNF-α expression (n=6). (E) Intracellular TNF-α levels (n=5). (F) qRT-PCR analysis of IL-1β expression (n=6). (G) Intracellular IL-1β levels (n=5). (H) Intracellular H_2O_2 levels (n=5). (I) Intracellular GSH levels (n=5). (J) Effect of GAs on ROS production in LPS-damaged NRK-52E cells. Scale bar: 100 μm. (K) Representative Western blots of Nrf2, HO-1, SLC7A11, GPX4, and FSP1 protein expression levels (n=3). (L) qRT-PCR analysis of Nrf2 expression (n=6). (M) qRT-PCR analysis of HO-1 expression (n=6). (N) qRT-PCR analysis of SLC7A11 expression (n=6). (O) qRT-PCR analysis of GPX4 expression (n=6). (P) qRT-PCR analysis of FSP1 expression (n=6). Data are shown as mean ± SEM. Statistical significance is indicated as $^{*}P < 0.05$, $^{**}P < 0.01$, and $^{***}P < 0.001$ versus the CTR group, and $^{\#}P < 0.05$, $^{\#\#}P < 0.01$, and $^{\#\#\#}P < 0.001$ versus the LPS group.

3.8. GA-C2 mediates Nrf2 by regulating the Keap-1 pathway and GSK3β pathway through targeting NEU1

GAs derived from *Ganoderma lucidum* exhibit pharmacological activity against neuraminidase [36]. We quantified neuraminidase levels in kidney tissue and cells, observing an increase in neuraminidase relative activity in comparison to the CTR group. Conversely, administration of GA-C2 resulted in a reduction of neuraminidase activity within both kidney tissue and cells (Fig. 8A and C). Importantly, GA-C2 demonstrated a significantly greater inhibitory effect on neuraminidase activity than Zanamivir, a neuraminidase inhibitor commonly used in clinical settings (Fig. 8C). Western blot analysis revealed that LPS stimulation elevated NEU1 expression in both cells and kidney tissue, whereas GA-C2 markedly decreased NEU1 expression levels (Fig. 8B and D). These findings were substantiated through immunohistochemical analysis, revealing a decrease in brown-positive areas in kidney sections treated with GA-C2 in comparison to those in the LPS group (Fig. 8E).

Following LPS stimulation, NRK-52E cells transfected with NC siRNA exhibited no significant background interference, confirming that the observed molecular changes were not attributable to nonspecific siRNA effects. In contrast, in NEU1-knockdown NRK-52E cells exposed to LPS, NEU1 expression was markedly reduced, whereas the expression levels of Nrf2, HO-1, SLC7A11, GPX4, FSP1, and IκBα were significantly upregulated. Moreover, phosphorylation of NF-κB was dysregulated, indicating an alteration in NF-κB signaling activity (Fig. 8F). Molecular docking analysis confirmed the specific binding of GA-C2 with NEU1, with a predicted binding energy lower than that of Zanamivir (Fig. 8G). To further validate their interaction, we performed CETSA, which demonstrated a difference in the denaturation temperature between NEU1 exposed to GA-C2 and NEU1 alone, indicating that GA-C2 directly binds to NEU1 (Fig. 8H). Co-IP assay revealed the binding of NEU1 to Keap-1 (Fig. 8I). Protein stability analysis showed that NEU1 knockout accelerated the degradation of Keap-1, leading to a reduction in its protein half-life (Fig. 8J). The knockdown of NEU1 led to the phosphorylation of Akt at the Ser473 residue, which in turn resulted in the phosphorylation of GSK3β at the Ser9 site. This phosphorylation event inhibited the interaction between Nrf2 and β-TrCP, thereby obstructing the subsequent ubiquitin-mediated degradation pathway (Fig. 8K). In summary, GA-C2 exerts a protective function by targeting NEU1 and regulating the Nrf2 pathway through the Keap-1 and GSK3β pathways.

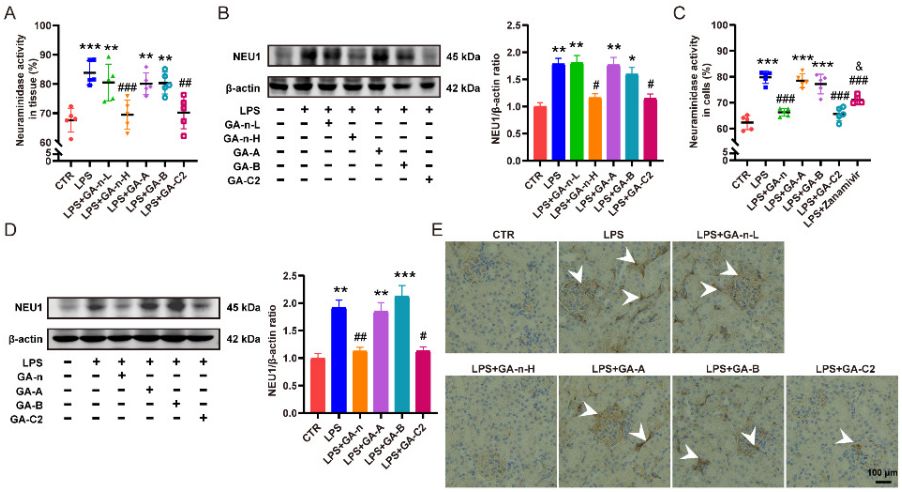

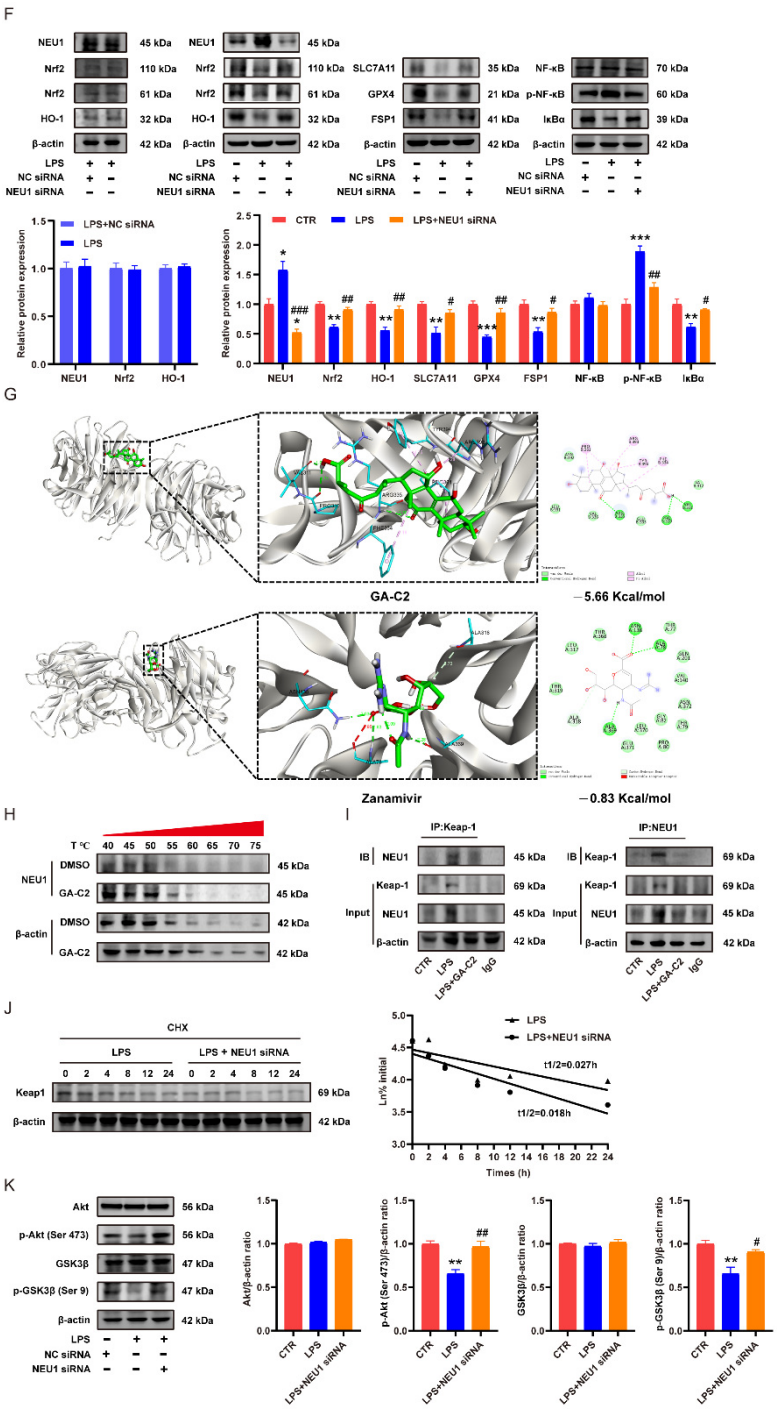

Fig. 8. GA-C2 targets NEU1 to regulate Nrf2 via the Keap-1 and GSK3β pathways. (A) Neuraminidase activity in kidney homogenates (n=5). (B) Representative Western blots showing NEU1 expression levels in kidney tissue (n=3). (C) Neuraminidase activity in NRK-52E cells (n=5). (D) Representative Western blots showing NEU1 expression levels in NRK-52E cells (n=3). (E) Immunohistochemistry staining of NEU1 in renal tissues. Scale bar: 100 μm. (F) Western blot analysis and quantification of NEU1, Nrf2, HO-1, SLC7A11, GPX4, FSP1, NF-κB, p-NF-κB, and IκBα protein expression in NRK-52E cells (n=3). (G) Molecular docking analysis illustrating the interaction between GA-C2 and NEU1 or Zanamivir. (H) CETSA assays confirming the binding of GA-C2 to NEU1 in NRK-52E cells. β-Actin was used as the internal control. (I) Co-IP analysis of NEU1 and Keap-1 interactions was performed in NRK-52E cells. Cells were assigned to three groups: untreated CTR, LPS treatment (1 μg/mL for 24 h), and combined treatment with LPS (1 μg/mL) and GA-C2 (25 μg/mL) for 24 h. Following treatment, cell lysates were collected and subjected to immunoprecipitation using either anti-Keap-1 or anti-NEU1 antibodies. Immunoprecipitated complexes were then analyzed by immunoblotting with the indicated antibodies. IgG was used as a negative control to exclude nonspecific binding. (J) Western blot analysis of Keap-1 protein half-life in NRK-52E cells following CHX (20 μg/mL) treatment at different time points (0, 2, 4, 8, 12, and 24 h). (K) Western blot analysis of protein kinase B (Akt), p-Akt (Ser473), GSK3β, and p-GSK3β (Ser9) protein expression in NRK-52E cells. Data are shown as mean ± SEM. Statistical significance is indicated as $^{*}P < 0.05$, $^{**}P < 0.01$, and $^{***}P < 0.001$ versus the CTR group, and $^{\#}P < 0.05$, $^{\#\#}P < 0.01$, and $^{\#\#\#}P < 0.001$ versus the LPS group, and $^{\&}P < 0.05$ versus the LPS + GA-C2 group.

4. Discussion

This study makes significant advancements in both the sustainable use of *Ganoderma lucidum* by-products and the understanding of GAs, particularly GA-C2, in the treatment of S-AKI. We present an eco-friendly approach for extracting high-purity GAs while revealing a novel regulatory pathway involving NEU1, Nrf2, and ferroptosis. This positions GA-C2 as a promising therapeutic agent. Our findings highlight the potential of GA-C2 in applications within the functional food and nutraceutical industries. In this discussion, we contextualize these developments within the broader fields of food chemistry and precision medicine.

GA-C2, the most potent isomer of GAs, exhibits dual properties of anti-ferroptosis and anti-inflammatory effects through a previously unidentified mechanism dependent on sialidase activity. Our experimental results demonstrate that GA-C2 has a higher binding affinity (-5.66 kcal/mol) for the catalytic pocket (ARG335/PRO310/VAL311) of NEU1 compared to Zanamivir (-0.83 kcal/mol), indicating its role as a novel NEU1 antagonist. This interaction disrupts NEU1's regulation of Nrf2 degradation through two distinct pathways: the Keap-1-dependent ubiquitination pathway and the GSK3β-driven phosphorylation pathway. In the Keap-1-dependent pathway, GA-C2 inhibits NEU1-mediated stabilization of Keap-1, promoting its proteasomal degradation and reducing Nrf2 ubiquitination. In the GSK3β-driven pathway, GA-C2 suppresses NEU1's inhibitory effect on Akt, leading to enhanced inactivation of GSK3β and blocking Nrf2 phosphorylation. Consequently, GA-C2 activates Nrf2, enhancing antioxidant defenses and suppressing ferroptosis. Additionally, GA-C2 down-regulates PTGS2 and MDA levels while restoring renal GSH content, thereby exhibiting anti-ferroptotic effects. These findings highlight the broad-spectrum regulatory capacity of GA-C2, positioning it as a "master regulator" of redox homeostasis. Supplementary, GA-C2 reduces p-NF-κB and increases IκBα expression, decreases TNF-α and IL-1β levels, thus exhibits anti-inflammatory effects. Moreover, they address the limitations of single-target therapies in the context of S-AKI. GA-C2's unique mechanism of action and its ability to simultaneously target multiple pathways make it a promising candidate for addressing the complex pathophysiology of S-AKI.

In the process of refining *Ganoderma lucidum* industrially, aqueous extracts are concentrated, resulting in insoluble residue at the bottom of the concentration vessel. Traditionally, this residue has been considered waste and discarded. However, our analysis revealed a significant concentration (15-20%) of bioactive GAs, including GA-A, GA-B, and GA-C2, within this residue. GAs, which are the key bioactive triterpenoids in *Ganoderma lucidum* [37], possess anti-inflammatory [22], antitumor [38], and immunomodulatory properties [39]. The isolation of GAs is challenging due to their structural homology, low natural abundance, and molecular diversity, leading to the high cost of obtaining purified standards. To address this, we have developed a streamlined protocol that combines aqueous extraction, concentration, and 10-kDa ultrafiltration, which helps retain the structural integrity of high-molecular-weight polysaccharide-peptides, thus improving yield and bioactivity. The fraction with a molecular weight below 10 kDa was precipitated using ethanol, followed by centrifugation and drying of the supernatant to obtain the crude GA-n (GAs-enriched fraction). To achieve

high purity, rapid purification chromatography was employed to isolate GA-A, GA-B, and GA-C2 from the GA-n fraction, resulting in a purity of over 98%. This method surpasses conventional techniques in terms of yield, purity, and preservation of the structural integrity of bioactive GAs. It enables scalable industrial production, offering a more efficient and cost-effective approach for obtaining bioactive GAs from *Ganoderma lucidum*.

Patients in the intensive care unit often experience the severe condition known as S-AKI [40], marked by rapid increases in serum creatinine or reduced urine output [41]. Conventional sepsis treatments, including antibiotics and vasoactive medications [42], may occasionally worsen kidney damage [43,44], highlighting the critical demand for new treatment approaches. In this study, we explore the therapeutic potential of GAs derived from *Ganoderma lucidum* for treating S-AKI. The key protective action of GAs is to activate the Nrf2 pathway by inhibiting NEU1, thereby reducing inflammation and preventing ferroptosis after oxidative stress. By lowering Keap-1 levels and enhancing p-GSK3β after NEU1 inhibition, GAs facilitate Nrf2 activation. This process alleviates oxidative stress in renal tubular epithelial cells, offering protection against iron-dependent ferroptosis, which plays a critical role in kidney injury. In addition, NEU1 inhibition reduced the inflammatory response by decreasing the phosphorylation of NF-κB and increasing IκBα levels. These findings suggest that GAs provide a promising therapeutic approach for treating S-AKI. By targeting dual mechanisms—reducing Keap-1 levels and increasing p-GSK3β to activate Nrf2 while inhibiting ferroptosis, diminishing pro-inflammatory cytokines—GAs could protect renal function and offer a novel treatment strategy for this devastating condition.

Natural antioxidants have drawn increasing attention for their protective roles against oxidative stress. A recent review by Wu et al. [45]highlighted the antioxidant effects of *Phyllanthus emblica* Linn. (PE), showing that its polyphenolic compounds can neutralize free radicals, prevent mitochondrial dysfunction, and inhibit lipid peroxidation. These actions contribute to delayed cellular aging and reduced incidence of age-related diseases. Our findings align with this broader context, demonstrating that GA-C2 effectively alleviates oxidative stress in S-AKI. This protective effect appears to be mediated by the activation of the Nrf2 pathway, leading to reduced ROS levels and inhibition of ferroptosis—both crucial in preserving renal function under septic conditions. The Nrf2 pathway serves as a central regulator of cellular redox homeostasis [46]. Under oxidative stress, Nrf2 activation induces the expression of antioxidant defense genes such as HO-1 and GPX4 [47]. Wu et al. [45]reported that PE enhances the body's antioxidative capacity through this same pathway. Similarly, our study found that GA-C2 not only stabilizes Nrf2 protein levels but also suppresses the activity of NEU1, a modulator of oxidative stress and inflammation. This dual mechanism—targeting both NEU1 inhibition and Nrf2 activation—amplifies antioxidant gene expression and curbs ferroptosis progression. Taken together, these findings suggest that GA-C2 offers a novel therapeutic approach for S-AKI by combining upstream inhibition of NEU1 with downstream activation of Nrf2-driven antioxidant responses. This integrated mechanism highlights the potential of GA-C2 as a multifaceted intervention in sepsis-related kidney injury.

GAs, the primary bioactive components found in *Ganoderma lucidum*, have gained significant attention due to their wide range of pharmacological properties [37]. These properties include anti-inflammatory [22], antioxidant [48], antidiabetic [48], anti-arthritic [49], anti-tumor [38], anti-aging [50], antimicrobial [51], immunomodulatory [39], cardioprotective [52], and organ-protective effects [22]. Previous studies have demonstrated the therapeutic potential of GAs in various conditions, such as lung injury [53], liver damage [54], and atherosclerosis [30]. Consistent with these previous findings, our research indicates that GAs offer protection against S-AKI by restoring kidney function and preventing pathological damage. The observed protective effect is likely due to the reduction of oxidative stress, inflammation, and ferroptosis, which are critical contributors to kidney injury. By utilizing their anti-inflammatory and antioxidant properties, GAs may mitigate the harmful effects of S-AKI, offering a potential therapeutic strategy for this condition. The capacity of GAs to modulate multiple pathways and address various facets of kidney injury underscores their potential as a comprehensive and effective treatment option for S-AKI.

Network pharmacology is an essential approach in understanding the complex interactions between GAs and their target molecules within the human body. In our study, we employed KEGG pathway enrichment analysis to gain insights into the therapeutic effects of GAs in S-AKI. We found that GAs' effects in S-AKI are associated with the regulation of ROS. The generation of ROS is a major factor in the pathogenesis of AKI [55]. Nrf2, a pivotal regulator of redox homeostasis, has been demonstrated to safeguard renal health by mitigating ROS levels [56], The activation of Nrf2 through specific compounds has been shown to effectively reduce ROS levels, thereby preventing or decelerating the progression of various AKI forms [57]. Our findings indicate that GAs may modulate oxidative stress induced by LPS and prevent S-AKI by influencing redox-related signaling pathways, aligning with existing literature. In our experimental validation, we concentrated on the Nrf2/HO-1 signaling pathway. Nrf2, as an essential transcription factor, is instrumental in regulating the expression of antioxidant genes and managing inflammation [58] as well as ferroptosis [59]. Our study confirms that GAs activate the Nrf2 pathway, leading to a reduction in ferroptosis and inhibition of inflammation. We further demonstrated the importance of Nrf2 signaling in protecting against S-AKI by observing that the anti-ferroptotic effects of GAs were significantly weakened when using the Nrf2-specific inhibitor ML385. In summary, our study demonstrates that GAs confer protective effects in S-AKI through the activation of the Nrf2 pathway, attenuation of ferroptosis, and suppression of inflammatory responses. These results underscore the potential of GAs as a therapeutic strategy for S-AKI, specifically by targeting critical pathways implicated in oxidative stress and renal damage.

This study concentrated on GA-C2, which has been identified as the most potent monomer among the GAs, demonstrating significant therapeutic effects on S-AKI. The pronounced efficacy of GA-C2 suggests its potential as a promising candidate for further research and possible clinical applications in the treatment of S-AKI. *Ganoderma* triterpenoids, characterized by their complex and highly oxidized chemical structures, can function as molecular probes for target proteins associated with specific activity sites [60]. Previous research has shown that *Ganoderma* triterpenoids, including GA-C2, possess the ability to inhibit neuraminidase

activity across various subtypes, with a particular affinity for N1 subtype [60]. Remarkably, NEU1, a unique form of neuraminidase, has been shown to block the PI3K-Akt signaling pathway [61]. In both *in vitro* and *in vivo* experiments, GA-C2 demonstrated the ability to inhibit NEU1 activity and reduce NEU1 expression. Molecular docking simulations indicated a stronger binding affinity between GA-C2 and NEU1 compared to Zanamivir, a known neuraminidase inhibitor. The binding of GA-C2 to the NEU1 catalytic site suggests its potential to effectively block NEU1's catalytic function. Moreover, GA-C2 was found to enhance the stability of the Nrf2 protein, leading to the activation of downstream antioxidant pathways such as HO-1 and GPX4. Additionally, GA-C2 was shown to suppress inflammatory factors like NF-κB. The protective effects of GA-C2 against S-AKI are supported by this interaction, which modulates oxidative stress, inflammation, and other significant pathways involved in kidney injury. Overall, the study highlights the therapeutic potential of GA-C2 in treating S-AKI through its multi-faceted mechanisms, including NEU1 inhibition, Nrf2 activation, and modulation of antioxidant and inflammatory pathways. These findings underscore the importance of GA-C2 as a promising therapeutic agent for S-AKI and warrant further investigation into its clinical applications.

This study underscores the therapeutic potential of GA-C2 in mitigating S-AKI. However, several limitations must be considered when interpreting these findings. First, the long-term efficacy of GA-C2 remains unclear. While our study primarily focused on the acute phase of kidney injury, it is crucial to determine whether GA-C2 can provide sustained renal protection over extended periods. Such data are essential for assessing its clinical applicability. Second, a more comprehensive dose-response analysis is necessary to identify the optimal therapeutic window, which could maximize efficacy while minimizing potential off-target effects. This step is pivotal for translating these findings into clinical settings. Third, additional control groups, such as vehicle-only treatments, should be incorporated in all experiments to further validate the mechanistic pathways identified in this study. Including these controls would help differentiate specific drug effects from experimental variability. Finally, replicating these findings in independent laboratories and utilizing alternative sepsis models, such as cecal ligation and puncture, would strengthen the robustness and generalizability of our conclusions. Despite these limitations, our findings lay a strong foundation for future research and highlight the translational promise of GA-C2 as a potential therapeutic agent for sepsis-induced kidney injury.

5. Conclusion

In summary, this study provides compelling evidence that GA-C2, a compound derived from *Ganoderma lucidum*, exerts a substantial effect on S-AKI by targeting NEU1, suppressing inflammatory responses, and modulating the Nrf2/ferroptosis axis (Fig. 9). By inhibiting NEU1 and activating Nrf2, GA-C2 reestablishes redox homeostasis and reduces ferroptosis, thereby offering a dual-target therapeutic strategy for S-AKI. Additionally, the study introduces an innovative extraction method for obtaining GAs from the by-products of *Ganoderma lucidum* processing, enhancing sustainability and cost-effectiveness in the production of these bioactive compounds. This research underscores the potential of *Ganoderma lucidum*-derived compounds,

such as GA-C2, in the development of functional foods and nutraceuticals. The findings pave the way for further research and clinical applications in the treatment of S-AKI. The dual-target therapeutic approach and the sustainable extraction process present promising opportunities for the application of *Ganoderma lucidum*-derived compounds in managing S-AKI and potentially other related conditions.

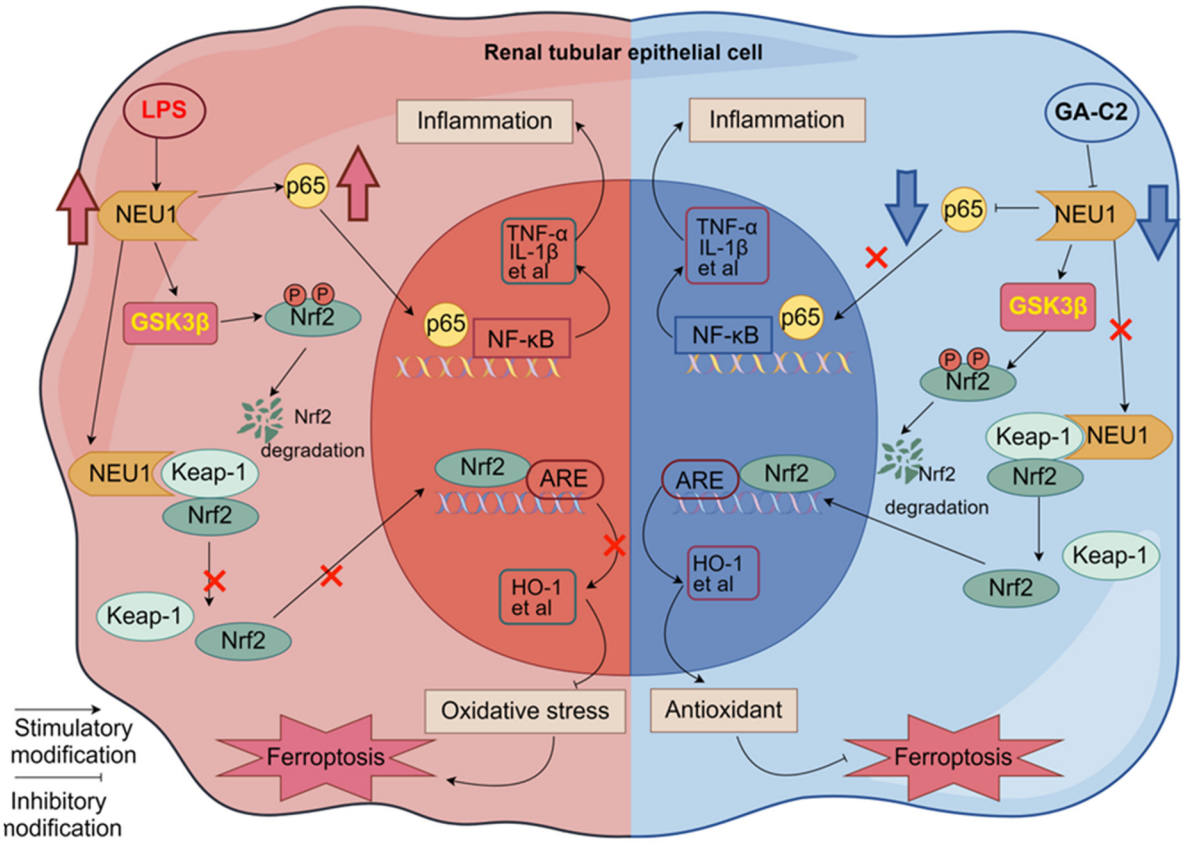

Fig. 9. This diagram illustrates the signaling pathways involved in LPS-induced S-AKI and the effect of GA-C2 (By Figdraw). In this study, we observed an increase in NEU1 levels following LPS treatment, which disrupted the interaction between Nrf2 and Keap-1, as well as the regulation of Nrf2 by GSK3β, leading to its ubiquitination and degradation. However, pretreatment with GA-C2 effectively reduced NEU1 levels, enhanced the antioxidant response, and alleviated renal tissue damage. Moreover, GA-C2 treatment decreased the phosphorylation of p65 and increased the expression of the IκBα protein. These findings suggest that GA-C2 inhibits NEU1, promoting the activation of Nrf2 and its downstream antioxidant genes, such as HO-1, to combat oxidative stress. Additionally, this inhibition suppresses the NF-κB pathway, ultimately reducing renal ferroptosis and mitigating renal injury.

Acknowledgments

This study received support from multiple funding sources. We are grateful for the grants provided by the National Natural Science Foundation of China (Grant No. 82000400 to H. Fang), the Weifang Science and Technology Development Plan (Grant No. 2025YX030 to H. Fang), the Special Project for the Protection and Utilization of Agricultural Resources from the Department of Agriculture and Rural Affairs of Fujian Province (Grant No. 22001XA to D. Lin), and the Science and Technology Innovation Special Fund Project of Fujian Agriculture and Forestry University (KFB24058 to D. Lin). The generous financial assistance from these organizations played a crucial role in the successful completion of this research.

Declaration of generative AI and AI-assisted technologies in the writing process

During this study, the authors utilized ChatGPT to improve the accuracy of spelling, grammar, coherence, and overall comprehensibility of the manuscript. They then meticulously reviewed and revised the material as needed, taking full responsibility for the content presented in this publication.

References

[1] Q. Peng, L. Zhang, Y. Ai, L. Zhang, Epidemiology of acute kidney injury in intensive care septic patients based on the KDIGO guidelines, Chin Med J (Engl) 127 (2014) 1820–1826. https://doi.org/10.3760/cma.j.issn.0366-6999.20140387.

[2] E.A.J. Hoste, J.A. Kellum, N.M. Selby, A. Zarbock, P.M. Palevsky, S.M. Bagshaw, S.L. Goldstein, J. Cerdá, L.S. Chawla, Global epidemiology and outcomes of acute kidney injury., Nat Rev Nephrol 14 (2018) 607–625. https://doi.org/10.1038/s41581-018-0052-0.

[3] S.M. Bagshaw, S. Uchino, R. Bellomo, H. Morimatsu, S. Morgera, M. Schetz, I. Tan, C. Bouman, E. Macedo, N. Gibney, A. Tolwani, H.M. Oudemans-van Straaten, C. Ronco, J.A. Kellum, Beginning and Ending Supportive Therapy for the Kidney (BEST Kidney) Investigators, Septic acute kidney injury in critically ill patients: clinical characteristics and outcomes., Clin J Am Soc Nephrol 2 (2007) 431–9. https://doi.org/10.2215/CJN.03681106.

[4] W. Zhang, H. Chen, Z. Xu, X. Zhang, X. Tan, N. He, J. Shen, J. Dong, Liensinine pretreatment reduces inflammation, oxidative stress, apoptosis, and autophagy to alleviate sepsis acute kidney injury., Int Immunopharmacol 122 (2023) 110563. https://doi.org/10.1016/j.intimp.2023.110563.

[5] Y. Ding, Y. Zheng, J. Huang, W. Peng, X. Chen, X. Kang, Q. Zeng, UCP2 ameliorates mitochondrial dysfunction, inflammation, and oxidative stress in lipopolysaccharide-induced acute kidney injury., Int Immunopharmacol 71 (2019) 336–349. https://doi.org/10.1016/j.intimp.2019.03.043.

[6] C. Su, Z. Liu, L. Liu, Z. Xiong, T. Xu, S. Zhang, Y. Chen, Y. Jiang, Protective effects of nodosin against lipopolysaccharide-induced acute kidney injury through regulation of oxidative stress, inflammation, and ferroptosis in rats., Naunyn Schmiedebergs Arch Pharmacol 397 (2024) 8009–8022. https://doi.org/10.1007/s00210-024-03148-x.

[7] W. Qiu, S. An, T. Wang, J. Li, B. Yu, Z. Zeng, Z. Chen, B. Lin, X. Lin, Y. Gao, Melatonin suppresses ferroptosis via activation of the Nrf2/HO-1 signaling pathway in the mouse model of sepsis-induced acute kidney injury., Int Immunopharmacol 112 (2022) 109162. https://doi.org/10.1016/j.intimp.2022.109162.

[8] J. Zhang, J. Jiang, B. Wang, Y. Wang, Y. Qian, J. Suo, Y. Li, Z. Peng, SAP130 released by ferroptosis tubular epithelial cells promotes macrophage polarization via Mincle signaling in sepsis acute kidney injury., Int Immunopharmacol 129 (2024) 111564. https://doi.org/10.1016/j.intimp.2024.111564.

[9] J. Du, H. Shui, R. Chen, Y. Dong, C. Xiao, Y. Hu, N.-K. Wong, Neuraminidase-1 (NEU1): Biological Roles and Therapeutic Relevance in Human Disease., Curr Issues Mol Biol 46 (2024) 8031–8052. https://doi.org/10.3390/cimb46080475.

[10] Q.-Q. Chen, K. Liu, N. Shi, G. Ma, P. Wang, H.-M. Xie, S.-J. Jin, T.-T. Wei, X.-Y. Yu, Y. Wang, J.-Y. Zhang, P. Li, L.-W. Qi, L. Zhang, Neuraminidase 1 promotes renal fibrosis development in male mice., Nat Commun 14 (2023) 1713. https://doi.org/10.1038/s41467-023-37450-8.

[11] K. Sundararaj, J. Rodgers, P. Angel, B. Wolf, T.K. Nowling, The role of neuraminidase in TLR4-MAPK signalling and the release of cytokines by lupus serum-stimulated mesangial cells., Immunology 162 (2021) 418–433. https://doi.org/10.1111/imm.13294.

[12] J. Rodgers, K. Sundararaj, E. Bruner, B. Wolf, T.K. Nowling, The role of neuraminidase 1 (NEU1) in cytokine release by primary mouse mesangial cells and disease outcomes in murine lupus nephritis., Autoimmunity 54 (2021) 163–175. https://doi.org/10.1080/08916934.2021.1897978.

[13] I.G. Luzina, E.P. Lillehoj, V. Lockatell, S.W. Hyun, K.N. Lugkey, A. Imamura, H. Ishida, C.W. Cairo, S.P. Atamas, S.E. Goldblum, Therapeutic Effect of Neuraminidase-1-Selective Inhibition in Mouse Models of Bleomycin-Induced Pulmonary Inflammation and Fibrosis., J Pharmacol Exp Ther 376 (2021) 136–146. https://doi.org/10.1124/jpet.120.000223.

[14] Z. Guo, H. Tuo, N. Tang, F.-Y. Liu, S.-Q. Ma, P. An, D. Yang, M.-Y. Wang, D. Fan, Z. Yang, Q.-Z. Tang, Neuraminidase 1 deficiency attenuates cardiac dysfunction, oxidative stress, fibrosis, inflammatory via AMPK-SIRT3 pathway in diabetic cardiomyopathy mice., Int J Biol Sci 18 (2022) 826–840. https://doi.org/10.7150/ijbs.65938.

[15] G.-P. Zhang, Y.-M. Pan, S.-M. Ye, Y.-C. Lu, X.-J. Fan, A.-Q. Zhang, Bioactive components of *Ganoderma lucidum* and their efficacy and application in cosmetics, Food & Medicine Homology 2 (2025) 9420044. https://doi.org/10.26599/FMH.2025.9420044.

[16] L.-Y. Wu, P.-P. Wu, X. Cheng, Y.-P. Chen, Q. Luo, Sesquiterpenoids and diterpenoids produced by *Ganoderma* species: structural diversity, biosynthesis, organic synthesis, and bioactivities, Food & Medicine Homology (2025). https://doi.org/10.26599/FMH.2026.9420111.

[17] Y. Xie, Y. Su, Y. Wang, D. Zhang, Q. Yu, C. Yan, Structural clarification of mannoglucan GSBP-2 from *Ganoderma sinense* and its effects on triple-negative breast cancer migration and invasion, Int J Biol Macromol 269 (2024) 131903. https://doi.org/10.1016/j.ijbiomac.2024.131903.

[18] Y.-K. Xie, X.-Y. Pan, X.-R. Liang, K.-F. Zhai, Q. Yu, Research progress on structural characterization and bioactivities of *Poria cocos* and *Ganoderma* polysaccharides, Food & Medicine Homology 2 (2025) 9420040. https://doi.org/10.26599/FMH.2025.9420040.

[19] C. Zheng, P. Rangsinth, P.H.T. Shiu, W. Wang, R. Li, J. Li, Y.-W. Kwan, G.P.H. Leung, A Review on the Sources, Structures, and Pharmacological Activities of Lucidenic Acids., Molecules 28 (2023). https://doi.org/10.3390/molecules28041756.

[20] W.-L. Guo, Y.-J. Cao, S.-Z. You, Q. Wu, F. Zhang, J.-Z. Han, X.-C. Lv, P.-F. Rao, L.-Z. Ai, L. Ni, Ganoderic acids-rich ethanol extract from *Ganoderma lucidum* protects against alcoholic liver injury and modulates intestinal microbiota in mice with excessive alcohol intake, Curr Res Food Sci 5 (2022) 515–530. https://doi.org/10.1016/j.crfs.2022.02.013.

[21] S. Peng, J. Qi, C. Lin, Z. Xu, Z. Li, C. Liu, From natural laboratory to drug discovery: Chemical structures, bioactivities, and biosynthesis of meroterpenoids from *Ganoderma* species, Chin Herb Med (2025). https://doi.org/10.1016/j.chmed.2025.03.003.

[22] G. Shao, J. He, J. Meng, A. Ma, X. Geng, S. Zhang, Z. Qiu, D. Lin, M. Li, H. Zhou, S. Lin, B. Yang, Ganoderic Acids Prevent Renal Ischemia Reperfusion Injury by Inhibiting Inflammation and Apoptosis., Int J Mol Sci 22 (2021). https://doi.org/10.3390/ijms221910229.

[23] C. Liang, D. Tian, Y. Liu, H. Li, J. Zhu, M. Li, M. Xin, J. Xia, Review of the molecular mechanisms of *Ganoderma lucidum* triterpenoids: Ganoderic acids A, C2, D, F, DM, X and Y., Eur J Med Chem 174 (2019) 130–141. https://doi.org/10.1016/j.ejmech.2019.04.039.

[24] H. Wu, S. Tang, Z. Huang, Q. Zhou, P. Zhang, Z. Chen, Hepatoprotective Effects and Mechanisms of Action of Triterpenoids from Lingzhi or Reishi Medicinal Mushroom *Ganoderma lucidum* (Agaricomycetes) on α-Amanitin-Induced Liver Injury in Mice, Int J Med Mushrooms 18 (2016) 841–850. https://doi.org/10.1615/IntJMedMushrooms.v18.i9.80.

[25] Q. Zheng, J. Xing, X. Li, X. Tang, D. Zhang, PRDM16 suppresses ferroptosis to protect against sepsis-associated acute kidney injury by targeting the NRF2/GPX4 axis., Redox Biol 78 (2024) 103417. https://doi.org/10.1016/j.redox.2024.103417.

[26] T. Li, Z. Geng, J. Zhang, L. Xu, X. Zhu, BP5 alleviates endotoxemia-induced acute lung injury by activating Nrf2 via dual regulation of the Keap1-Nrf2 interaction and the Akt (Ser473)/GSK3β (Ser9)/Fyn pathway., Free Radic Biol Med 193 (2022) 304–318. https://doi.org/10.1016/j.freeradbiomed.2022.10.299.

[27] L. Ni, C. Yuan, X. Wu, Targeting ferroptosis in acute kidney injury., Cell Death Dis 13 (2022) 182. https://doi.org/10.1038/s41419-022-04628-9.

[28] Y. Chen, Z. Jiang, X. Li, New insights into crosstalk between Nrf2 pathway and ferroptosis in lung disease., Cell Death Dis 15 (2024) 841. https://doi.org/10.1038/s41419-024-07224-1.

[29] P.-M. Psefteli, P. Kitscha, G. Vizcay, R. Fleck, S.J. Chapple, G.E. Mann, M. Fowler, R.C. Siow, Glycocalyx sialic acids regulate Nrf2-mediated signaling by fluid shear stress in human endothelial cells., Redox Biol 38 (2021) 101816. https://doi.org/10.1016/j.redox.2020.101816.

[30] Y.-Z. Quan, A. Ma, C.-Q. Ren, Y.-P. An, P.-S. Qiao, C. Gao, Y.-K. Zhang, X.-W. Li, S.-M. Lin, N.-N. Li, D.-L. Chen, Y. Pan, H. Zhou, D.-M. Lin, S.-Q. Lin, M. Li, B.-X. Yang, Ganoderic acids alleviate atherosclerosis by inhibiting macrophage M1 polarization via TLR4/MyD88/NF-κB signaling pathway., Atherosclerosis 391 (2024) 117478. https://doi.org/10.1016/j.atherosclerosis.2024.117478.

[31] T. Yang, H. Fang, D. Lin, S. Yang, H. Luo, L. Wang, B. Yang, *Ganoderma Lucidum* polysaccharide peptide (GL-PP2): A potential therapeutic agent against sepsis-induced organ injury by modulating Nrf2/NF-κB pathways., Int J Biol Macromol 285 (2025) 138378. https://doi.org/10.1016/j.ijbiomac.2024.138378.

[32] H. Fang, D. Lin, X. Li, L. Wang, T. Yang, Therapeutic potential of *Ganoderma lucidum* polysaccharide peptide in Doxorubicin-induced nephropathy: modulation of renin-angiotensin system and proteinuria., Front Pharmacol 14 (2023) 1287908. https://doi.org/10.3389/fphar.2023.1287908.

[33] H. Fang, X. Li, D. Lin, L. Wang, T. Yang, B. Yang, Inhibition of intrarenal PRR-RAS pathway by *Ganoderma lucidum* polysaccharide peptides in proteinuric nephropathy., Int J Biol Macromol 253 (2023) 127336. https://doi.org/10.1016/j.ijbiomac.2023.127336.

[34] H. Fang, C. Xu, A. Lu, C.-J. Zou, S. Xie, Y. Chen, L. Zhou, M. Liu, L. Wang, W. Wang, T. Yang, (Pro)renin receptor mediates albumin-induced cellular responses: role of site-1 protease-derived soluble (pro)renin receptor in renal epithelial cells., Am J Physiol Cell Physiol 313 (2017) C632–C643. https://doi.org/10.1152/ajpcell.00006.2017.

[35] Y. Liu, S. Wang, G. Jin, K. Gao, S. Wang, X. Zhang, K. Zhou, Y. Cai, X. Zhou, Z. Zhao, Network pharmacology-based study on the mechanism of ShenKang injection in diabetic kidney disease through Keap1/Nrf2/Ho-1 signaling pathway., Phytomedicine 118 (2023) 154915. https://doi.org/10.1016/j.phymed.2023.154915.

[36] Z. Yang, F. Wu, X. Yuan, L. Zhang, S. Zhang, Novel binding patterns between ganoderic acids and neuraminidase: Insights from docking, molecular dynamics and MM/PBSA studies., J Mol Graph Model 65 (2016) 27–34. https://doi.org/10.1016/j.jmgm.2016.02.006.

[37] M.F. Ahmad, S. Wahab, F.A. Ahmad, S.A. Ashraf, S.S. Abullais, H.H. Saad, *Ganoderma lucidum*: A potential pleiotropic approach of ganoderic acids in health reinforcement and factors influencing their production, Fungal Biol Rev 39 (2022) 100–125. https://doi.org/10.1016/j.fbr.2021.12.003.

[38] X.-L. Wang, Z.-Y. Ding, G.-Q. Liu, H. Yang, G.-Y. Zhou, Improved Production and Antitumor Properties of Triterpene Acids from Submerged Culture of *Ganoderma lingzhi*., Molecules 21 (2016). https://doi.org/10.3390/molecules21101395.

[39] Y. Liu, D. Tan, H. Cui, J. Wang, Ganoderic acid C2 exerts the pharmacological effects against cyclophosphamide-induced immunosuppression: a study involving molecular docking and experimental validation., Sci Rep 13 (2023) 17745. https://doi.org/10.1038/s41598-023-44394-y.

[40] Y. Chen, H. Jing, S. Tang, P. Liu, Y. Cheng, Y. Fan, H. Chen, J. Zhou, Non-Coding RNAs in Sepsis-Associated Acute Kidney Injury., Front Physiol 13 (2022) 830924. https://doi.org/10.3389/fphys.2022.830924.

[41] T. Li, J. Zhang, M. Long, X. Jiang, C. Yang, F. Wang, L. Su, Z. Peng, Macrophage Migration Inhibitory Factor Provides a Predictive Performance of Septic Acute Kidney Injury., Shock 57 (2022) 666–671. https://doi.org/10.1097/SHK.0000000000001918.

[42] J.-L. Vincent, Current sepsis therapeutics., EBioMedicine 86 (2022) 104318. https://doi.org/10.1016/j.ebiom.2022.104318.

[43] T. Chinzowu, T.-Y. Chyou, P.S. Nishtala, Antibiotic-Associated Acute Kidney Injury Among Older Adults: A Case-Crossover Study., Clin Drug Investig 44 (2024) 131–139. https://doi.org/10.1007/s40261-023-01339-7.

[44] M. Deniz, M. Alişik, Risk factors and prognosis for the development of acute kidney injury in patients using colistin in the intensive care unit: A retrospective cohort study, Medicine 103 (2024) e36913. https://doi.org/10.1097/MD.0000000000036913.

[45] N. Wu, Y. Pan, Q. Liu, F. Shahidi, H.-Y. Li, F. Chen, Z.-Y. Deng, Z.-H. Zhang, Protective benefits and mechanisms of *Phyllanthus emblica* Linn. on aging induced by oxidative stress: a system review, Food & Medicine Homology 2 (2025) 9420029. https://doi.org/10.26599/FMH.2025.9420029.

[46] J. Sivinski, D.D. Zhang, E. Chapman, Targeting NRF2 to treat cancer, Semin Cancer Biol 76 (2021) 61–73. https://doi.org/10.1016/j.semcancer.2021.06.003.

[47] K. Shen, X. Wang, Y. Wang, Y. Jia, Y. Zhang, K. Wang, L. Luo, W. Cai, J. Li, S. Li, Y. Du, L. Zhang, H. Zhang, Y. Chen, C. Xu, J. Zhang, R. Wang, X. Yang, Y. Wang, D. Hu, miR-125b-5p in adipose derived stem cells exosome alleviates pulmonary microvascular endothelial cells ferroptosis via Keap1/Nrf2/GPX4 in sepsis lung injury., Redox Biol 62 (2023) 102655. https://doi.org/10.1016/j.redox.2023.102655.

[48] D.H. Ryu, J.Y. Cho, N. Bin Sadiq, J.-C. Kim, B. Lee, M. Hamayun, T.S. Lee, H.S. Kim, S.H. Park, C.W. Nho, H.-Y. Kim, Optimization of antioxidant, anti-diabetic, and anti-inflammatory activities and ganoderic acid content of differentially dried *Ganoderma lucidum* using response surface methodology., Food Chem 335 (2021) 127645. https://doi.org/10.1016/j.foodchem.2020.127645.

[49] W. Wu, K. Song, G. Chen, N. Liu, T. Cao, Ganoderic acid A improves osteoarthritis by regulating RANKL/OPG ratio., Chem Biol Drug Des 100 (2022) 313–319. https://doi.org/10.1111/cbdd.14101.

[50] H. Yuan, Y. Xu, Y. Luo, J.-R. Zhang, X.-X. Zhu, J.-H. Xiao, Ganoderic acid D prevents oxidative stress-induced senescence by targeting 14-3-3ε to activate CaM/CaMKII/NRF2 signaling pathway in mesenchymal stem cells., Aging Cell 21 (2022) e13686. https://doi.org/10.1111/acel.13686.

[51] W. Zhang, W. Yu, X. Ding, C. Yin, J. Yan, E. Yang, F. Guo, D. Sun, W. Wang, Self-assembled thermal gold nanorod-loaded thermosensitive liposome-encapsulated ganoderic acid for antibacterial and cancer photochemotherapy., Artif Cells Nanomed Biotechnol 47 (2019) 406–419. https://doi.org/10.1080/21691401.2018.1559177.

[52] Y. Zhang, K. Shi, T. Lin, F. Xia, Y. Cai, Y. Ye, L. Liu, F. Liu, Ganoderic acid A alleviates myocardial ischemia-reperfusion injury in rats by regulating JAK2/STAT3/NF-κB pathway., Int Immunopharmacol 84 (2020) 106543. https://doi.org/10.1016/j.intimp.2020.106543.

[53] J. Shi, H. Wang, J. Liu, Y. Zhang, J. Luo, Y. Li, C. Yang, J. Jiang, Ganoderic acid B attenuates LPS-induced lung injury., Int Immunopharmacol 88 (2020) 106990. https://doi.org/10.1016/j.intimp.2020.106990.

[54] Y.-J. Cao, Z.-R. Huang, S.-Z. You, W.-L. Guo, F. Zhang, B. Liu, X.-C. Lv, Z.-X. Lin, P.-H. Liu, The Protective Effects of Ganoderic Acids from *Ganoderma lucidum* Fruiting Body on Alcoholic Liver Injury and Intestinal Microflora Disturbance in Mice with Excessive Alcohol Intake., Foods 11 (2022). https://doi.org/10.3390/foods11070949.

[55] L. Su, J. Zhang, H. Gomez, J.A. Kellum, Z. Peng, Mitochondria ROS and mitophagy in acute kidney injury., Autophagy 19 (2023) 401–414. https://doi.org/10.1080/15548627.2022.2084862.

[56] B. Bao, H. Liu, Y. Han, L. Xu, W. Xing, Z. Li, Simultaneous Elimination of Reactive Oxygen Species and Activation of Nrf2 by Ultrasmall Nanoparticles to Relieve Acute Kidney Injury., ACS Appl Mater Interfaces 15 (2023) 16460–16470. https://doi.org/10.1021/acsami.3c00052.

[57] W. Wei, N. Ma, X. Fan, Q. Yu, X. Ci, The role of Nrf2 in acute kidney injury: Novel molecular mechanisms and therapeutic approaches., Free Radic Biol Med 158 (2020) 1–12. https://doi.org/10.1016/j.freeradbiomed.2020.06.025.

[58] N. Ma, W. Wei, X. Fan, X. Ci, Farrerol Attenuates Cisplatin-Induced Nephrotoxicity by Inhibiting the Reactive Oxygen Species-Mediated Oxidation, Inflammation, and Apoptotic Signaling Pathways., Front Physiol 10 (2019) 1419. https://doi.org/10.3389/fphys.2019.01419.

[59] R. Yan, B. Lin, W. Jin, L. Tang, S. Hu, R. Cai, NRF2, a Superstar of Ferroptosis, Antioxidants 12 (2023) 1739. https://doi.org/10.3390/antiox12091739.

[60] Q. Zhu, T.H. Bang, K. Ohnuki, T. Sawai, K. Sawai, K. Shimizu, Inhibition of neuraminidase by *Ganoderma* triterpenoids and implications for neuraminidase inhibitor design., Sci Rep 5 (2015) 13194. https://doi.org/10.1038/srep13194.

[61] S.W. Hyun, A. Imamura, H. Ishida, K.H. Piepenbrink, S.E. Goldblum, E.P. Lillehoj, The sialidase NEU1 directly interacts with the juxtamembranous segment of the cytoplasmic domain of mucin-1 to inhibit downstream PI3K-Akt signaling., J Biol Chem 297 (2021) 101337. https://doi.org/10.1016/j.jbc.2021.101337.